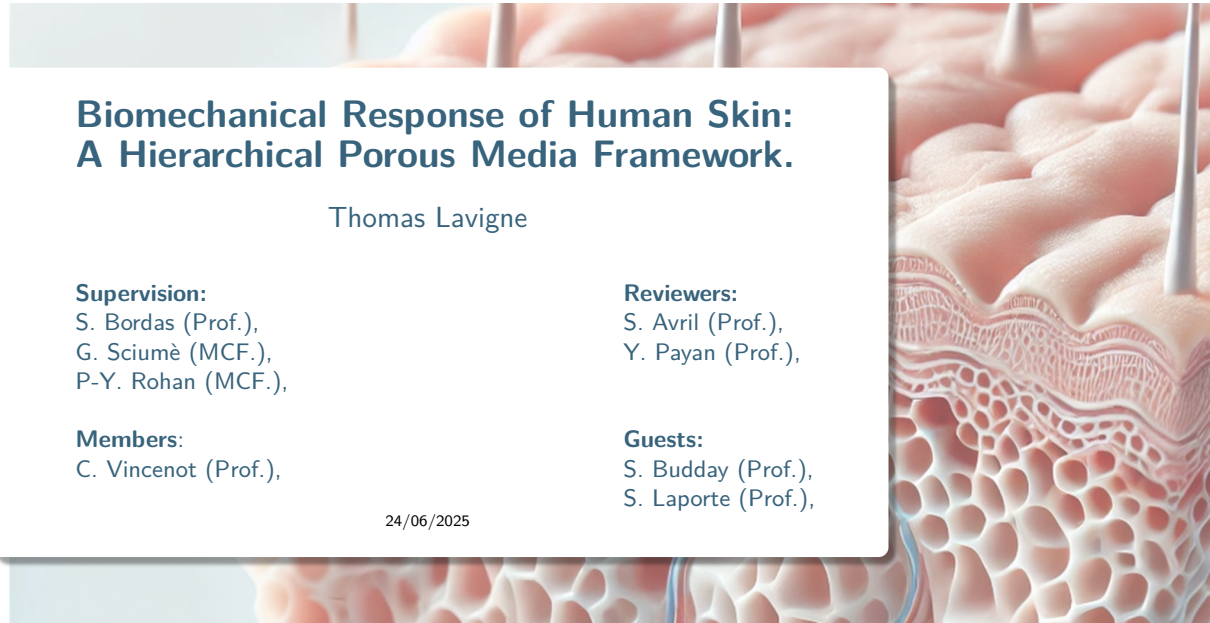

Biomechanical Response of Human Skin: A Hierarchical Porous Media Framework.

Thomas Lavigne

Supervision:
S. Bordas (Prof.),
G. Sciumè (MCF.),
P-Y. Rohan (MCF.),

Reviewers:
S. Avril (Prof.),
Y. Payan (Prof.),

Members:
C. Vincenot (Prof.),

Guests:
S. Budday (Prof.),
S. Laporte (Prof.),

24/06/2025

Context

Pressure ulcers:
a preventable tissue injury?

Pressure Ulcers (PUs)

Pressure ulcers: localised injuries to the skin and underlying soft tissue that form during **prolonged exposure** to mechanical loads [NPIAP].

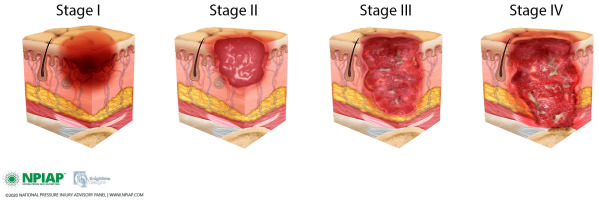

Pressure Ulcers (PUs)

Pressure ulcers: localised injuries to the skin and underlying soft tissue that form during **prolonged exposure** to mechanical loads [NPIAP].

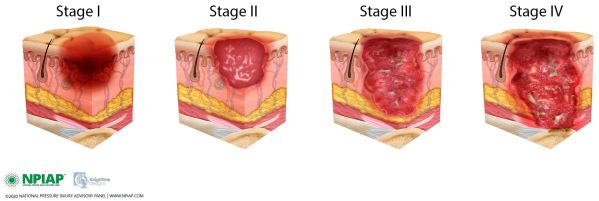

- Stage 1 and stage 2 account for **70%** of PUs

  [Kim et al., 2020, Moore et al., 2019],

Pressure Ulcers (PUs)

Pressure ulcers: localised injuries to the skin and underlying soft tissue that form during **prolonged exposure** to mechanical loads [NPIAP].

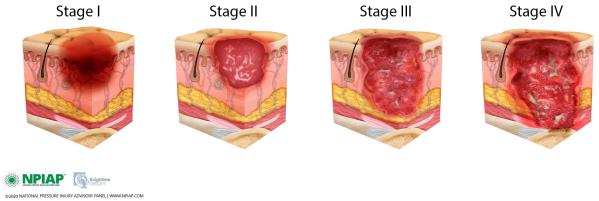

- Stage 1 and stage 2 account for **70%** of PUs
  [Kim et al., 2020, Moore et al., 2019],
- **20%** of hospitalised patients
  [Vanderwee et al., 2007],

Pressure Ulcers (PUs)

Pressure ulcers: localised injuries to the skin and underlying soft tissue that form during **prolonged exposure** to mechanical loads [NPIAP].

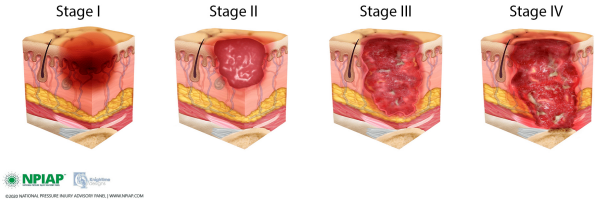

- Stage 1 and stage 2 account for **70%** of PUs [Kim et al., 2020, Moore et al., 2019],
- **20%** of hospitalised patients [Vanderwee et al., 2007],
- **34%** of amputees experienced a skin lesion [Lyon et al., 2000].

Challenges for the prevention of PUs

Clinical Challenges:

- ☞ Early detection of skin damage to enforce preventive measures: **Reliability** of PU risk assessment scales [Anthony et al., 2008],

Challenges for the prevention of PUs

Clinical Challenges:

- ☞ Early detection of skin damage to enforce preventive measures: **Reliability** of PU risk assessment scales [Anthony et al., 2008],
- ☞ Identification of at risk persons: Overall there is **no single factor** which can explain PU risk, rather a complex interplay of factors [Coleman et al., 2013],

Challenges for the prevention of PUs

Clinical Challenges:

- ☞ Early detection of skin damage to enforce preventive measures: **Reliability** of PU risk assessment scales [Anthony et al., 2008],
- ☞ Identification of at risk persons: Overall there is **no single factor** which can explain PU risk, rather a complex interplay of factors [Coleman et al., 2013],
- ☞ Healing processes are costly: prevention measures are five times less expensive than treating pressure ulcers [Demarré et al., 2015].

PUs prevention: clinical reality

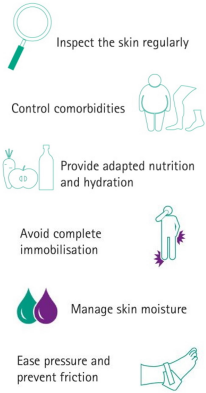

dermolex

Braden scale

Sensory perception It measures the ability to respond meaningfully to pressure-related discomfort.	**Mobility** Ability to change body position.
Moisture How often and to what extent is the patient's body exposed to moisture?	**Nutrition** Usual food intake pattern.
Activity Degree of physical activity	**Friction and shear** How often does the patient's skin rub?

Norton and Braden scores.

PUs prevention: clinical research

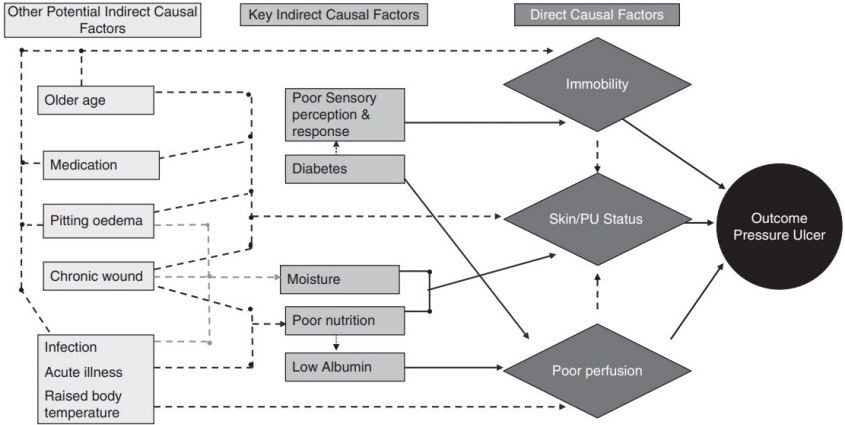

[Coleman et al., 2014]

PUs prevention: clinical research

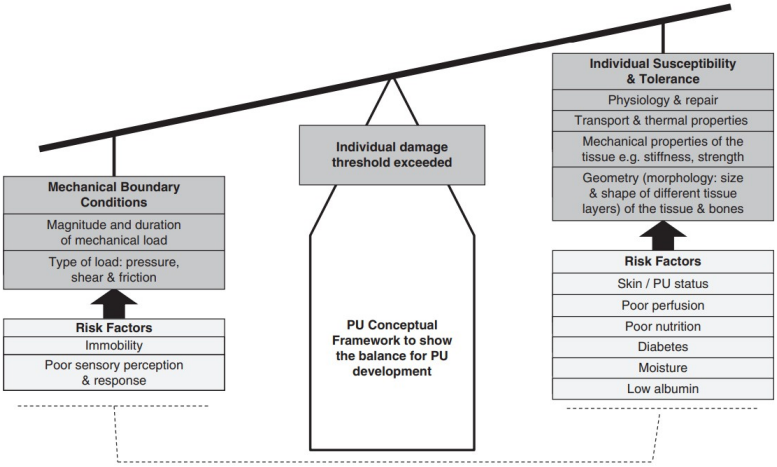

[Coleman et al., 2014]

PUs prevention: pre-clinical studies

Mechanical loading

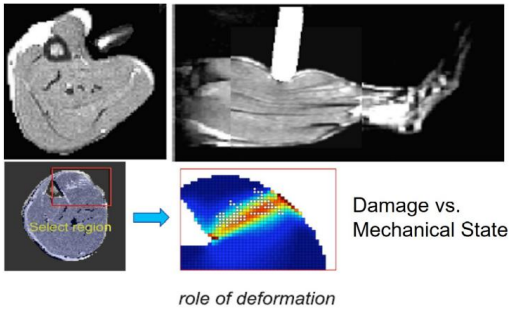

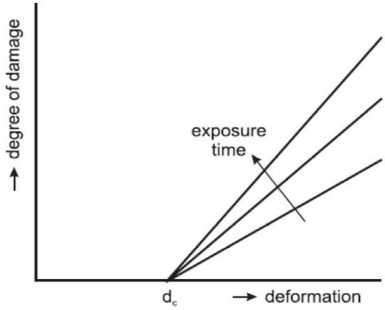

[Coleman et al., 2014, Ceelen et al., 2008, Traa et al., 2019, Loerakker et al., 2011, Stekelenburg et al., 2006, Bouten et al., 2003]

PUs prevention: pre-clinical studies

Skin Status

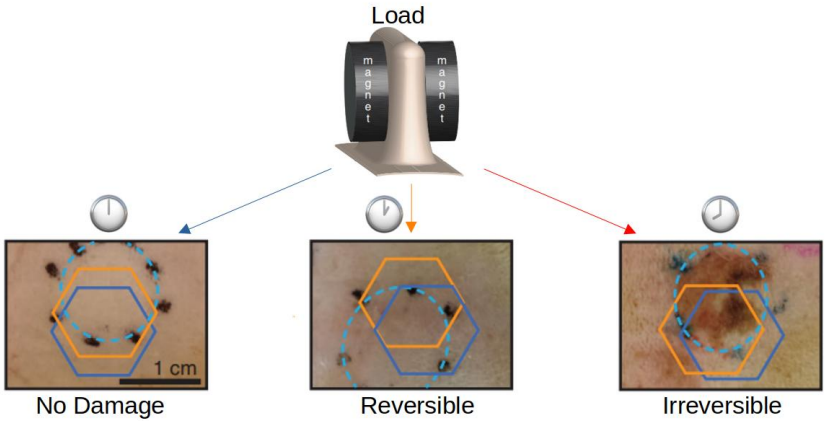

[Coleman et al., 2014, Swisher et al., 2015]

PUs prevention: pre-clinical studies

Perfusion

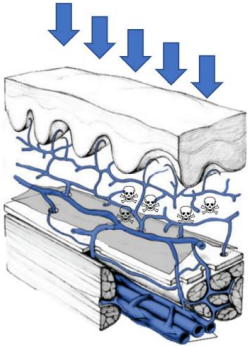

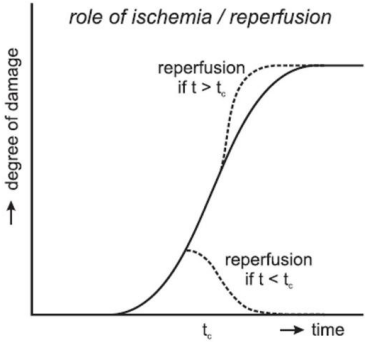

[Coleman et al., 2014, Kosiak, 1959, Landis, 1930, Loerakker et al., 2011]

PUs prevention: Interplay often overlooked

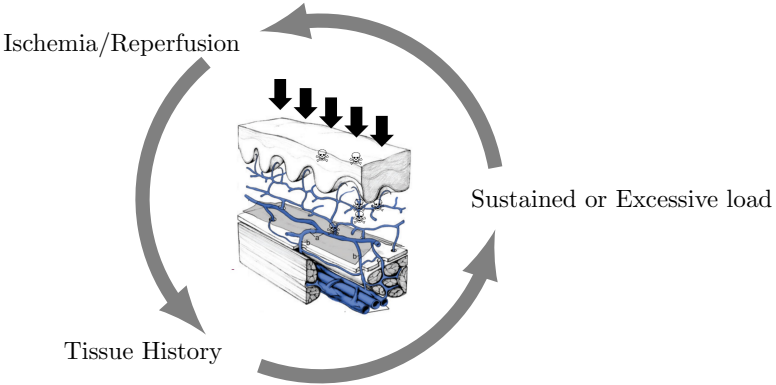

Literature review

Clinical, experimental and mathematical description of the human skin.

Clinical description of the skin

The human skin is the largest organ of the body ($\approx 7.00\,\%$ of the weight [Burns et al., 2010]). It is a **stratified tissue** acting as a barrier with the environment, ensuring load bearing, healing, and thermoregulation.

The main layers are:

- Epidermis (0.05-0.15mm): avascularised tissue [Burns et al., 2010, Wong et al., 2015, Joodaki and Panzer, 2018, Yazdi and Baqersad, 2022],

Clinical description of the skin

The human skin is the largest organ of the body ($\approx 7.00\,\%$ of the weight [Burns et al., 2010]). It is a **stratified tissue** acting as a barrier with the environment, ensuring load bearing, healing, and thermoregulation.

The main layers are:

- Epidermis (0.05-0.15mm): avascularised tissue [Burns et al., 2010, Wong et al., 2015, Joodaki and Panzer, 2018, Yazdi and Baqersad, 2022],
- Dermis (0.5-5mm): vascularised and fibrous system. 60% of Dermis weight is Bounded+Free water [Burns et al., 2010, Yazdi and Baqersad, 2022],

Clinical description of the skin

The human skin is the largest organ of the body ($\approx 7.00\,\%$ of the weight [Burns et al., 2010]). It is a **stratified tissue** acting as a barrier with the environment, ensuring load bearing, healing, and thermoregulation.

The main layers are:

- Epidermis (0.05-0.15mm): avascularised tissue [Burns et al., 2010, Wong et al., 2015, Joodaki and Panzer, 2018, Yazdi and Baqersad, 2022],
- Dermis (0.5-5mm): vascularised and fibrous system. 60% of Dermis weight is Bounded+Free water [Burns et al., 2010, Yazdi and Baqersad, 2022],
- Subcutaneous fat (subcutis): organised layer ensuring load bearing, and thermoregulation [Burns et al., 2010].

Clinical description of the skin

The human skin is the largest organ of the body ($\approx 7.00\,\%$ of the weight [Burns et al., 2010]). It is a **stratified tissue** acting as a barrier with the environment, ensuring load bearing, healing, and thermoregulation.

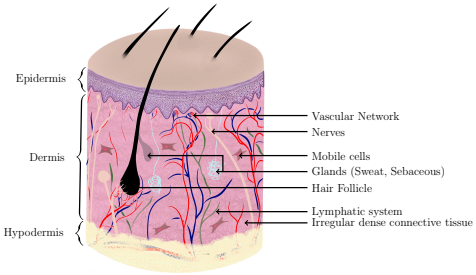

The main layers are:

- Epidermis (0.05-0.15mm): avascularised tissue [Burns et al., 2010, Wong et al., 2015, Joodaki and Panzer, 2018, Yazdi and Baqersad, 2022],
- Dermis (0.5-5mm): vascularised and fibrous system. 60% of Dermis weight is Bounded+Free water [Burns et al., 2010, Yazdi and Baqersad, 2022],
- Subcutaneous fat (subcutis): organised layer ensuring load bearing, and thermoregulation [Burns et al., 2010].

Mechanics of human skin

Tensile test	*In vivo* / *Ex vivo*
[Khatyr et al., 2004]	*In vivo*
[Annaidh et al., 2012]	*Ex vivo*
[Gallagher et al., 2012]	*Ex vivo*
[Ottenio et al., 2015]	*Ex vivo*
[Jacquet et al., 2017]	*In vivo*
Torsion test	*In vivo* / *Ex vivo*
[Sanders, 1973]	*In vivo*
[Agache et al., 1980]	*In vivo*
[Escoffier et al., 1989]	*In vivo*
Suction test	*In vivo* / *Ex vivo*
[Diridollou et al., 2000]	*In vivo*
[Hendriks et al., 2003]	*In vivo*
[Lakhani et al., 2021]	*In vivo*
[Connesson et al., 2023]	*In vivo*
[Elouneg et al., 2023]	*In vivo*
Indentation test	*In vivo* / *Ex vivo*
[Raveh Tilleman et al., 2004]	*Ex vivo*
[Elleuch et al., 2006]	*In vivo*
[Boyer et al., 2007]	*In vivo*
[Pailler-Mattei et al., 2008]	*In vivo*
[Khaothong, 2010]	*In vivo*

[Joodaki and Panzer, 2018]

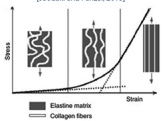

[Elouneg et al., 2023]

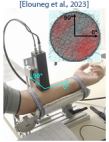

[Khatyr et al., 2004]

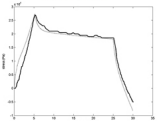

The human skin's mechanical response exhibits an **non-linear**, **anisotropic**, and **time-dependent** behaviour.

- Various experimental conditions,

Mechanics of human skin

Tensile test	*In vivo* / *Ex vivo*	Elastic Modulus [Pa]	Poisson Ratio [-]
[Khatyr et al., 2004]	*In vivo*	$(6.57 \pm 2.19) \times 10^5$ (∥ arm) $(1.3 \pm 0.62) \times 10^5$ (⊥ arm)	N-S
[Annaidh et al., 2012]	*Ex vivo*	$(83.3 \pm 34.9) \times 10^6$	N-S
[Gallagher et al., 2012]	*Ex vivo*	$(98.97 \pm 97) \times 10^6$	0.1-1.1
[Ottenio et al., 2015]	*Ex vivo*	$(76.7 \pm 40.3) \times 10^6$ ($0.06s^{-1}$) $(104.4 \pm 44.7) \times 10^6$ ($53s^{-1}$) $\mathbf{(169.1 \pm 70.5) \times 10^6}$ ($167s^{-1}$)	N-S
[Jacquet et al., 2017]	*In vivo*	$(56.58 \pm 13.27) \times 10^3$ (Initial) $(2.24 \pm 0.48) \times 10^6$ (Final) $(18.3 \pm 7.8) \times 10^3$ (Initial) $(0.74 \pm 0.59) \times 10^6$ (Final) $\mathbf{35.6 \times 10^3}$ (Initial) 4.59×10^6 (Final)	N-S
Torsion test	*In vivo* / *Ex vivo*	Elastic Modulus [Pa]	Poisson Ratio [-]
[Sanders, 1973]	*In vivo*	2×10^4 to 1×10^5	0.5
[Agache et al., 1980]	*In vivo*	4.2×10^5 (Young) 8.5×10^5 (Elderly)	N-S
[Escoffier et al., 1989]	*In vivo*	1.12×10^6	N-S
Suction test	*In vivo* / *Ex vivo*	Elastic Modulus [Pa]	Poisson Ratio [-]
[Diridollou et al., 2000]	*In vivo*	$(129 \pm 88) \times 10^3$	0.5
[Hendriks et al., 2003]	*In vivo*	$(56.3 \pm 20.4) \times 10^3$ N-S	N-S
[Lakhani et al., 2021]	*In vivo*	$(0.52 \pm 0.09) \times 10^6$ (Initial) $(3.09 \pm 0.47) \times 10^6$(Final)	0.5
[Connesson et al., 2023]	*In vivo*	$(53.5 \pm 1.05) \times 10^3$ $(4.8 \pm 0.1) \times 10^3$	0.45-0.5
[Elouneg et al., 2023]	*In vivo*	$(1.35 \pm 0.65) \times 10^6$ (∥ arm) $(0.43 \pm 0.07) \times 10^6$ (⊥ arm)	0.43 ± 0.09
Indentation test	*In vivo* / *Ex vivo*	Elastic Modulus [Pa]	Poisson Ratio [-]
[Raveh Tilleman et al., 2004]	*Ex vivo*	$52 \pm 45 \times 10^3$	0.43 ± 0.12
[Elleuch et al., 2006]	*In vivo*	14×10^3	0.3
[Boyer et al., 2007]	*In vivo*	13.2×10^3 to 33.4×10^3 N-S	N-S N-S
[Pailler-Mattei et al., 2008]	*In vivo*	35×10^3 2×10^3	N-S N-S
[Khaothong, 2010]	*In vivo*	$(0.17 \pm 0.07) \times 10^6$	N-S

The human skin's mechanical response exhibits an **non-linear**, **anisotropic**, and **time-dependent** behaviour.

- Various experimental conditions,
- Different modelling strategies,
- Wide range of values ($E \in [1e3, 1e6]$Pa).

Time-dependent mechanical response

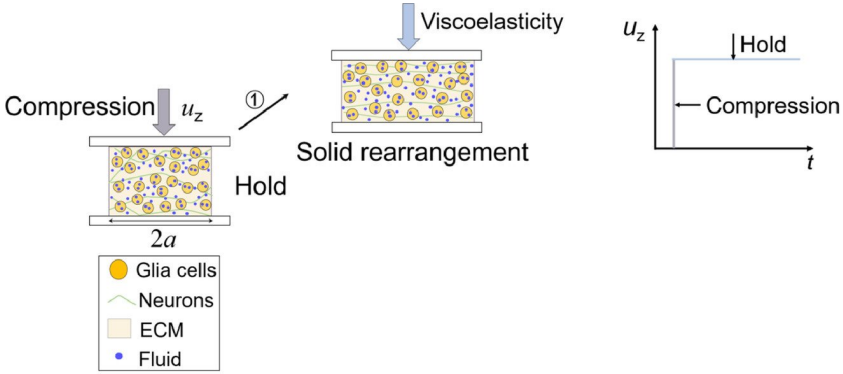

[Su et al., 2023] (Brain tissue)

Time-dependent mechanical response

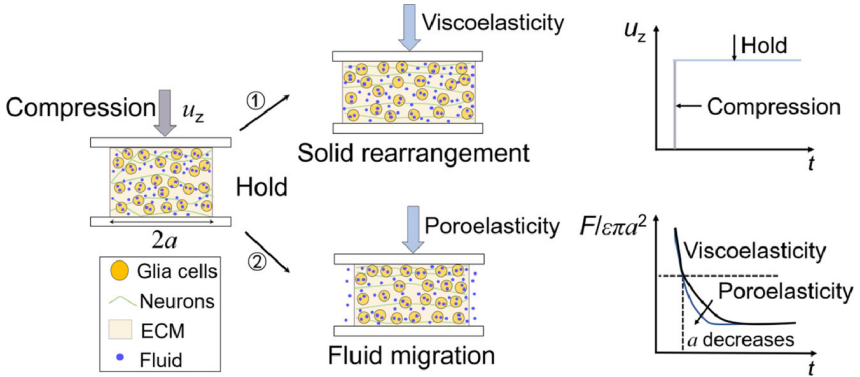

[Su et al., 2023] (Brain tissue)

Porous media description for human skin

Poromechanical models **allow the coupling** of the solid phase with the fluid compartments where biochemistry exchanges occur.

Tissue	Study
Brain	[Budday et al., 2019, Hosseini-Farid et al., 2020, Greiner et al., 2021, Urcun et al., 2021, Urcun et al., 2022, Urcun et al., 2023], [Hervas-Raluy et al., 2023, Carrasco-Mantis et al., 2023]
Liver	[Jordan et al., 2009, Marchesseau et al., 2010, Raghunathan et al., 2010, Moran et al., 2012] [Ricken and Lambers, 2019, Islam et al., 2020]
Meniscus	[Kazemi et al., 2013, Uzuner et al., 2020, Bulle, 2022, Uzuner et al., 2022, Gunda et al., 2023, Schwer et al., 2024]
Muscle	[Yang and Taber, 1991, Morrow et al., 2012, Wheatley et al., 2015, Wheatley et al., 2016, Lavigne et al., 2022]
Skin	[Oomens et al., 1987, Ehlers and Markert, 2001, Nakagawa et al., 2010, Oftadeh et al., 2018, Wahlsten et al., 2019], [Wang et al., 2020, Leng et al., 2021, Sachs et al., 2021, de Lucio et al., 2023, Oftadeh et al., 2023, Han et al., 2023], [Sachs et al., 2024, de Lucio et al., 2024]

Porous media description for human skin

There's a chemo-mechanical coupling at play: Water movement—driven by osmotic pressure and chemical potential—regulates how the tissue adapts to deformation by compacting or expanding the collagen fiber network. [Ehret et al., 2017]

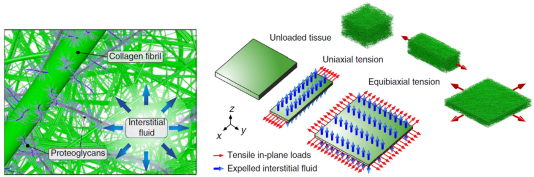

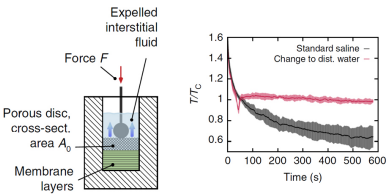

Uniaxial tension relaxation experiments on human amnion.

Porous media description for human skin

Biphasic homogenized model and experiments [Wahlsten et al., 2019]

Ex vivo characterisation

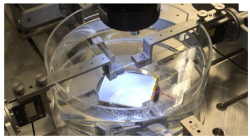

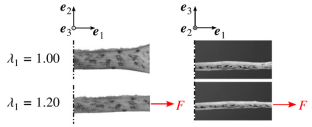

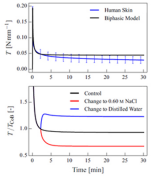

In vivo predictions

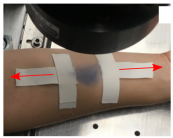

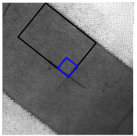

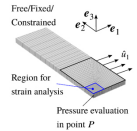

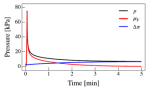

Porous media description for human skin

Expansion to layer-specific biphasic model for skin [Sachs et al., 2021]: stiffer dermis and key role of fluid flow and permeability in the tissue's mechanical response.

Layered biphasic model

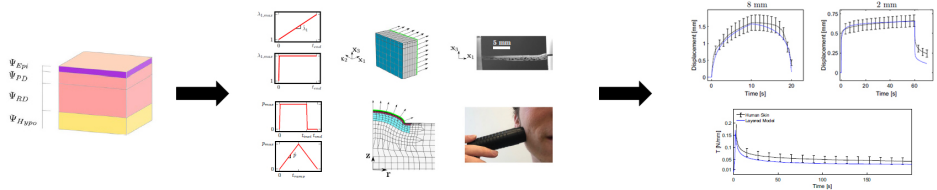

Porous media description for human skin

Expansion to quadriphasic model for dermis [Sachs et al., 2024].

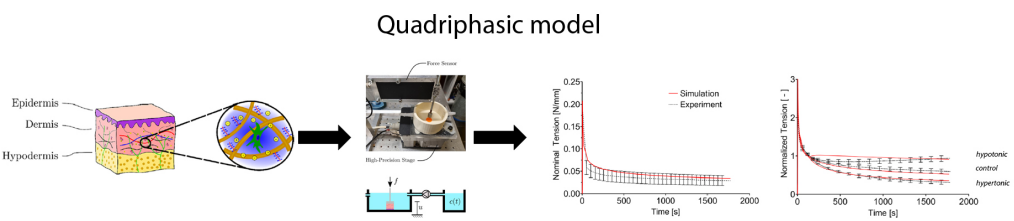

Porous media description for human skin

Current limitations

- Few ***in vivo*** studies have been published and **evaluated** for skin [Oomens et al., 1987, Weir Weiss et al., 2023, Sachs et al., 2021],
- Limited **loading** or **boundary condition** is controlled [Wahlsten et al., 2019, Wahlsten et al., 2023],
- Few studies have examined the **interplay** between identified factors and included the **vascular system** [Sree et al., 2019, Loerakker et al., 2011]
- Multi-compartment poromechanical models including the vascular system **have not been evaluated yet**.

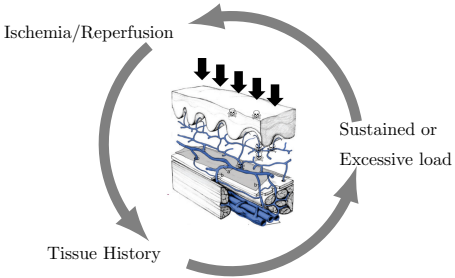

Current approaches for vascular coupling

Explicit and FE^{2}modelling

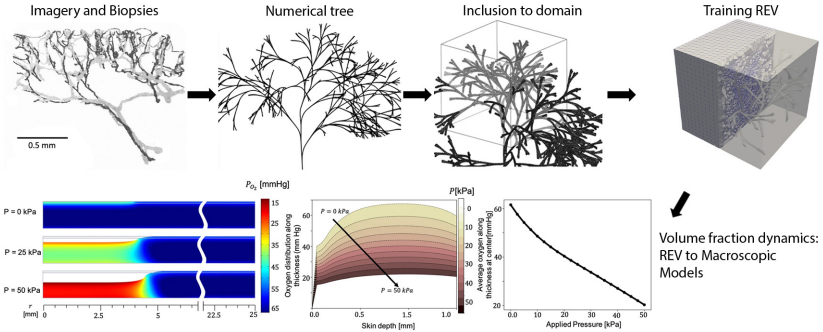

[Sree et al., 2019] ($\approx 1,210,000$ elements)

Porous media description for living tissues

This PhD work is built upon the Theory of Thermodynamically Constrained Averaging Theory (**TCAT**, [Gray and Miller, 2014]) and Sciumè et al., Urcun et al. adaptations to ulceration and oncophysics.

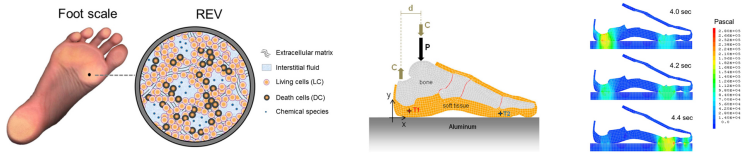

[Sciumè et al., 2014, Sciumè, 2021, Urcun et al., 2022, Urcun et al., 2023].

Objectives

Develop and evaluate a poromechanical model that couples mechanical behaviour and micro-circulation.

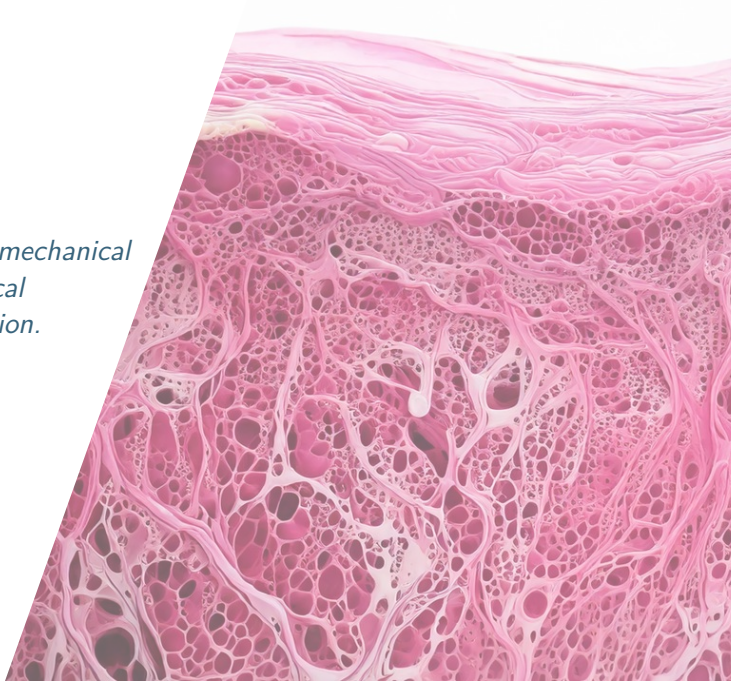

Modular poromechanical model

Challenges

- How can we introduce the vascular system to a poromechanical model for the skin?
- How can we evaluate the poromechanical model with the vascular system?

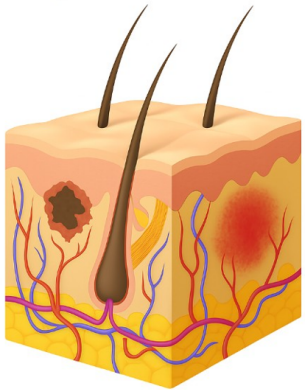

Generated with AI

Modular poromechanical model

Challenges

- How can we introduce the vascular system to a poromechanical model for the skin?
- How can we evaluate the poromechanical model with the vascular system?

Remark

PUs are associated with damage (tissue necrosis). In this project, we focus on the **interplay** between mechanics and biological response. Therefore, we first consider physiological mechanical ranges.

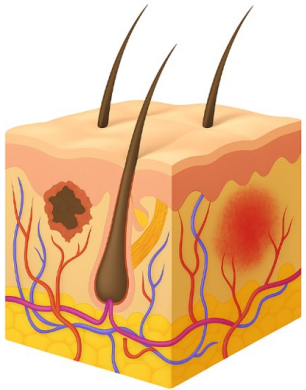

Generated with AI

Porous Modelling

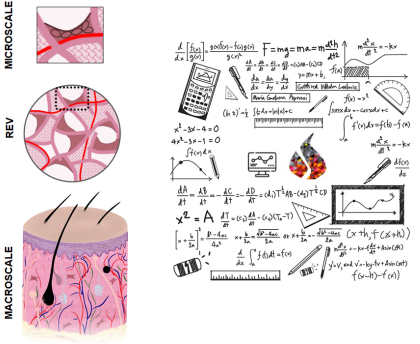

Porous Modelling

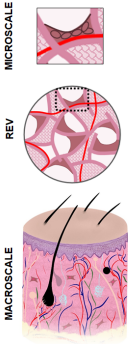

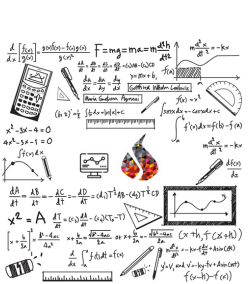

Model Evaluation

Tensile Test

FEniCSx Integration

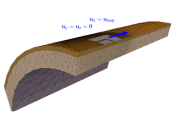

Evaluation of the model

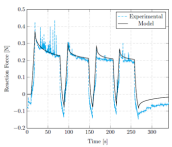

Porous Modelling

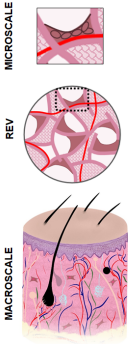

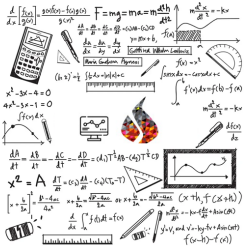

Model Evaluation

Tensile Test

FEniCSx Integration

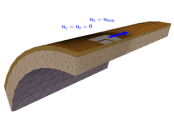

Evaluation of the model

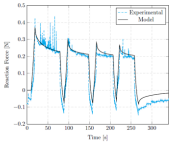

LDF Experiments

FEniCSx Integration

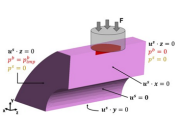

Evaluation of the model

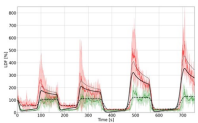

Model developments

☞ How can we introduce the vascular system to a poromechanical model for the skin?

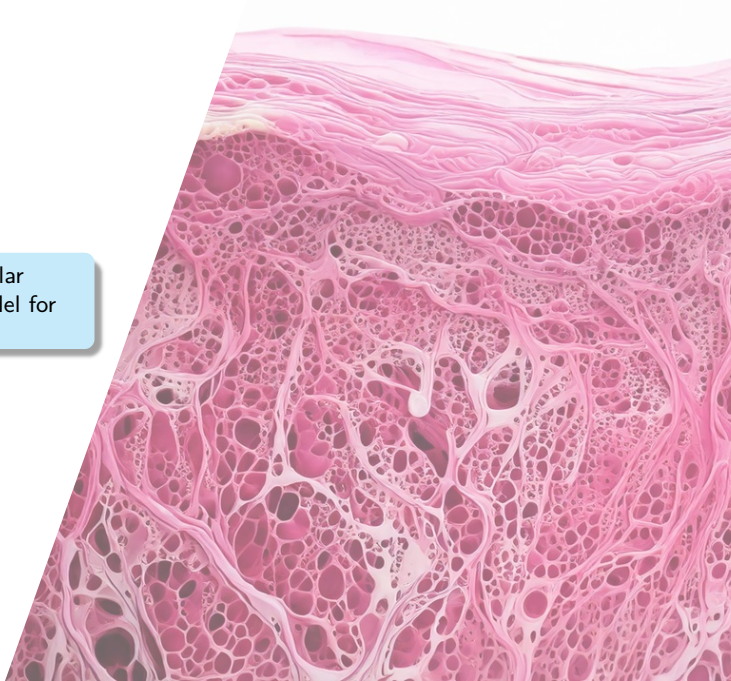

Poromechanical systems

A **system** is a **quantity of mass**. The complement of a system, *i.e.* the mass or region outside the system, is the **surrounding**. (*Nonlinear Solid Mechanics*, Holzapfel 2000)

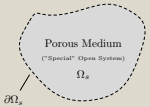

A porous medium: special Open System in which the control volume, Ω_s , is that occupied by the solid scaffold. Being the solid deformable Ω_s and $\partial\Omega_s$ **depends on time** t.

Poromechanical systems

A **system** is a **quantity of mass**. The complement of a system, *i.e.* the mass or region outside the system, is the **surrounding**. (*Nonlinear Solid Mechanics*, Holzapfel 2000)

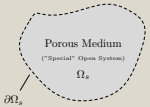

A porous medium: special Open System in which the control volume, Ω_s , is that occupied by the solid scaffold. Being the solid deformable Ω_s and $\partial\Omega_s$ **depends on time** t.

Material derivative:

$$\frac{\mathrm{D}^\alpha f^\pi}{\mathrm{D}t} = \frac{\partial f^\pi}{\partial t} + \nabla f^\pi \cdot \mathbf{v}^\alpha$$

The description of phases' motion is:

- **material** for the solid phase,
- **spatial** for the fluid phases.

In other words, the deforming solid scaffold is the reference space where the fluid phases' motion is described in a spatial way.

Porous medium analogy

Volume fraction constraint:

$$\sum_{\alpha} \varepsilon^{\alpha} = 1 \ (100\%)$$

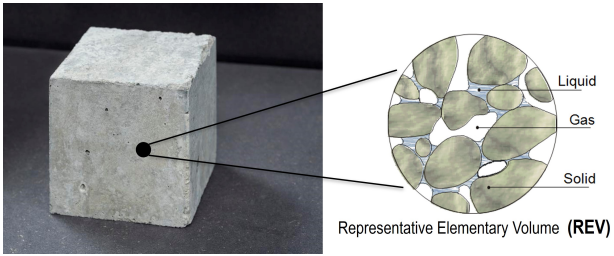

Porous medium analogy

Volume fraction constraint:

$$\sum_{\alpha} \varepsilon^{\alpha} = 1 \ (100\%)$$

The behaviour is governed by:

- ➢ Conservation equations of mass,
- ➢ Conservation equations of momentum,
- \+ Chemical reaction equations.
- ➢ Unknowns of the problem: p^f, u^s

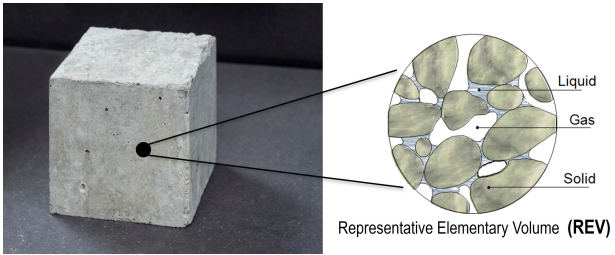

Porous medium analogy

Volume fraction constraint:

$$\varepsilon^{solid} + \underbrace{\varepsilon^{liquid} + \varepsilon^{cell}}_{\varepsilon} + \varepsilon^{blood} = 1$$

ε: extra-vascular porosity

The behaviour is governed by:

- ➢ Conservation equations of mass,
- ➢ Conservation equations of momentum,
- \+ Chemical reaction equations.
- ➢ Unknowns of the problem: p^f, u^s

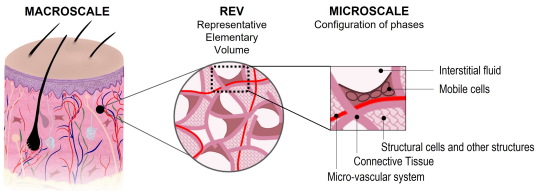

- ➢ Two **coupled** and **deformable** compartments (extended Biot's theory),
- ➢ Large strain regime.

Phases description

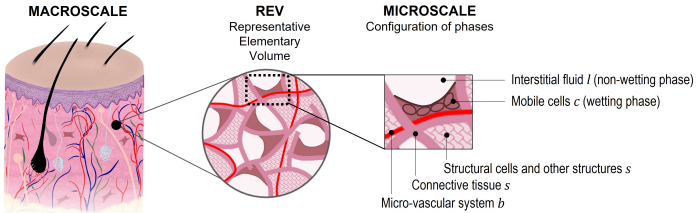

Phase \ Species	Connective Tissue	Other structures (glands, hair, etc.)	Mobile Cells	Water	Oxygen	Other Species
Solid (s)	✓	✓		✓		✓
Liquid (l)				✓	✓	✓
Cell (c)			✓	✓	✓	✓
Vascular (blood) (b)				✓	✓	✓

Mechanical parameters

Parameter (symbol)	Physics
Young's modulus (E)	Stiffness of the solid
Poisson's ratio (ν)	Influence the compressibility
Intrinsic permeability (k^l, k^c, k^b)	The ability of the medium to conduct fluids
Fluid viscosity (μ^l, μ^c, μ^b)	Force needed to overcome internal friction in a fluid
Fluid conductivity (L^l, L^c, L^b)	Ratio $L^\alpha = \frac{k^\alpha}{\mu^\alpha}$
Extra-vascular porosity (ε)	Volume fraction corresponding to the interstitium
Vascular porosity (ε^b)	Volume fraction occupied by the blood
Vessel Compressibility (K)	Relative change in the volume of a body produced by a unit load.

Mechanical parameters

Parameter (symbol)	Physics
Young's modulus (E)	Stiffness of the solid
Poisson's ratio (ν)	Influence the compressibility
Intrinsic permeability (k^l, k^c, k^b)	The ability of the medium to conduct fluids
Fluid viscosity (μ^l, μ^c, μ^b)	Force needed to overcome internal friction in a fluid
Fluid conductivity (L^l, L^c, L^b)	Ratio $L^\alpha = \frac{k^\alpha}{\mu^\alpha}$
Extra-vascular porosity (ε)	Volume fraction corresponding to the interstitium
Vascular porosity (ε^b)	Volume fraction occupied by the blood
Vessel Compressibility (K)	Relative change in the volume of a body produced by a unit load.

Mechanical parameters

Parameter (symbol)	Physics
Young's modulus (E)	Stiffness of the solid
Poisson's ratio (ν)	Influence the compressibility
Intrinsic permeability (k^l, k^c, k^b)	The ability of the medium to conduct fluids
Fluid viscosity (μ^l, μ^c, μ^b)	Force needed to overcome internal friction in a fluid
Fluid conductivity (L^l, L^c, L^b)	Ratio $L^\alpha = \frac{k^\alpha}{\mu^\alpha}$
Extra-vascular porosity (ε)	Volume fraction corresponding to the interstitium
Vascular porosity (ε^b)	Volume fraction occupied by the blood
Vessel Compressibility (K)	Relative change in the volume of a body produced by a unit load.

Conservation Laws

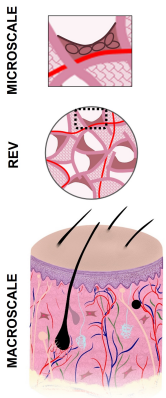

Poromechanical model

Conservation Laws

Continuity Equation (Mass)

Solid | Mobile Cells

IF | Blood | Oxygen

Momentum Conservation

Total stress

Darcy IF | Darcy Blood | Darcy Cells

Unknowns: u^s, p^f

Constitutive Laws

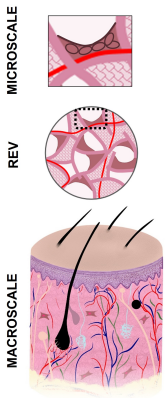

Poromechanical model

Conservation Laws

Continuity Equation (Mass)

Solid | Mobile Cells

IF | Blood | Oxygen

Momentum Conservation

Total stress

Darcy IF | Darcy Blood | Darcy Cells

Constitutive Laws

Solid

Stress-Strain law

Interstitium

saturation-capillary pressure

Vascular Phase

Porosity | Permeability

Oxygen

Diffusion O_2 | Absorption O_2

Unknowns: u^s, p^f

Hypotheses

Hypothesis 1: Blood **vessels interact primarily with fluid** constituents, and so they have no significant effect on the "structural" connective tissue fibres.

Hypotheses

Hypothesis 1: Blood **vessels interact primarily with fluid** constituents, and so they have no significant effect on the "structural" connective tissue fibres.

Hypothesis 2: The **solid pressure** (averaged effect of the fluid on the solid), p^s, is assumed to be **related** to the pressure of the fluids in the **extravascular space** only.

Vascular porosity state equation

Hypothesis 3: Consistently with hypothesis 1, we suppose that ε^b depends on $(p^s - p^b)$.

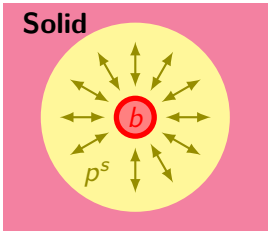

Vascular porosity state equation

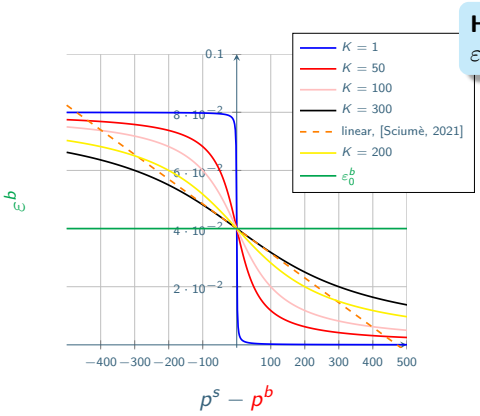

Hypothesis 3: Consistently with hypothesis 1, we suppose that ε^b depends on $(p^s - p^b)$.

$$\varepsilon^b = \varepsilon_0^b \cdot \left(1 - \frac{2}{\pi} \arctan\left(\frac{p^s - p^b}{K}\right)\right) \qquad (1)$$

Unkowns / Material Parameters

Vascular porosity state equation

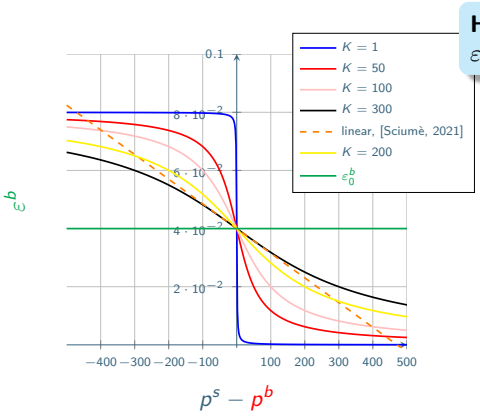

Hypothesis 3: Consistently with hypothesis 1, we suppose that ε^b depends on $(p^s - p^b)$.

$$\varepsilon^b = \varepsilon_0^b \cdot \left(1 - \frac{2}{\pi} \arctan\left(\frac{p^s - p^b}{K}\right)\right) \quad (1)$$

Similarly, we can introduce:

$$k^b = k_0^b \cdot \left(\frac{\varepsilon^b}{\varepsilon_0^b}\right)^\alpha, \ \alpha \geq 2 \quad (2)$$

Vascular porosity state equation

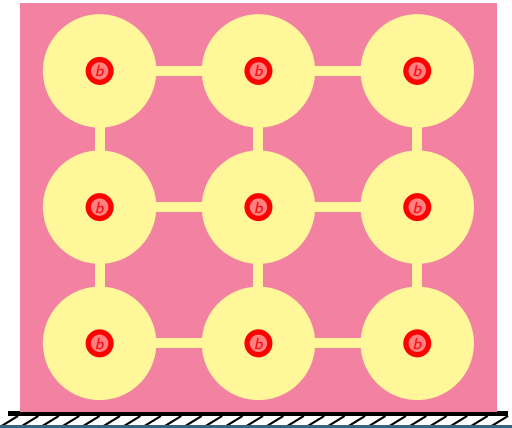

"How does it work?"

The solid scaffold interacts with the blood vessels via the extravascular fluids.

Vascular porosity state equation

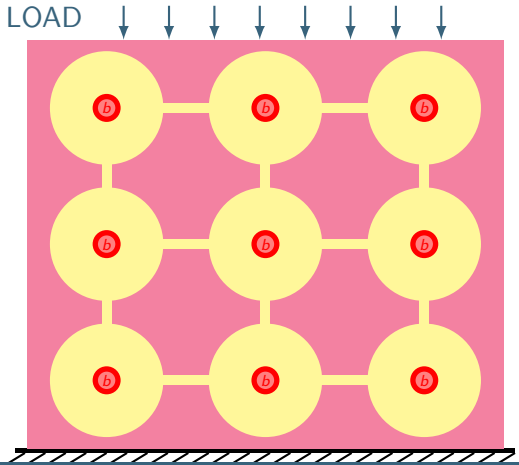

"How does it work?"

The solid scaffold interacts with the blood vessels via the extravascular fluids.

Vascular porosity state equation

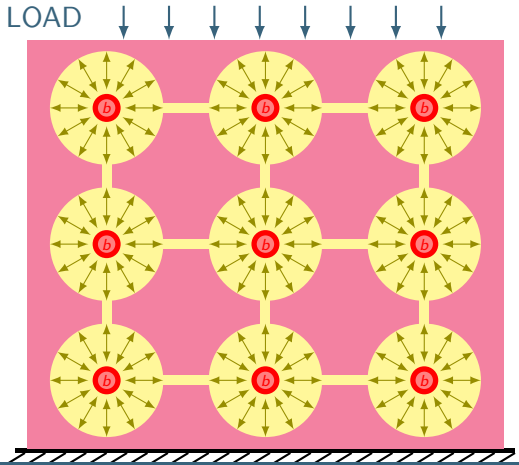

"How does it work?"

The solid scaffold interacts with the blood vessels via the extravascular fluids.

1D Consolidation Column

A first test case of a 1D consolidation was tested on a column using FEniCSx.

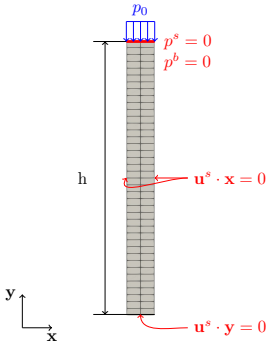

1D Consolidation Column

A first test case of a 1D consolidation was tested on a column using FEniCSx.

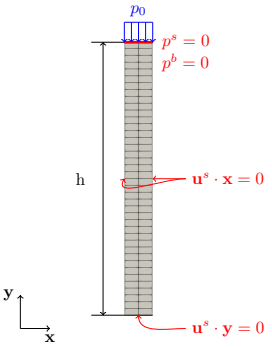

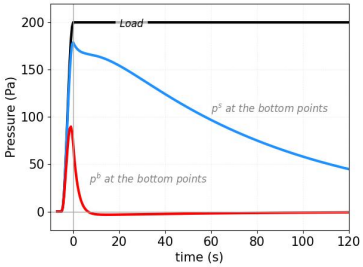

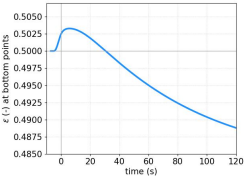

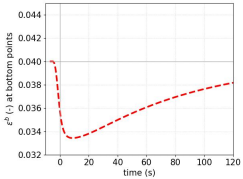

—— $\varepsilon = \varepsilon^I$;

1D Consolidation Column

A first test case of a 1D consolidation was tested on a column using FEniCSx.

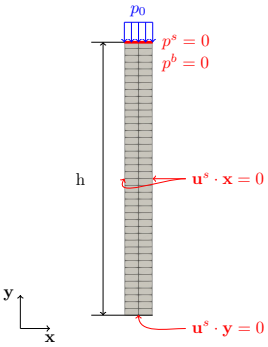

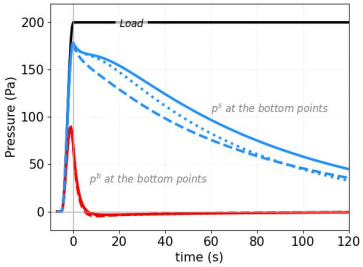

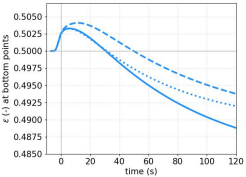

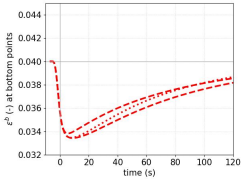

—— $\varepsilon = \varepsilon^l$;
$\varepsilon^l/\varepsilon$ =85%; $\varepsilon^c/\varepsilon$ =15%: - - - $\mu^c = 1$Pa s; ····· $\mu^c = 5$Pa s;

1D Consolidation Column

A first test case of a 1D consolidation was tested on a column using FEniCSx.

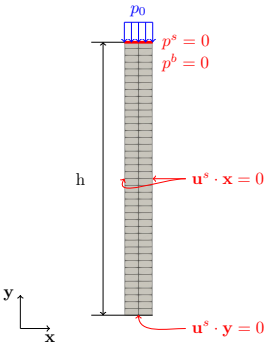

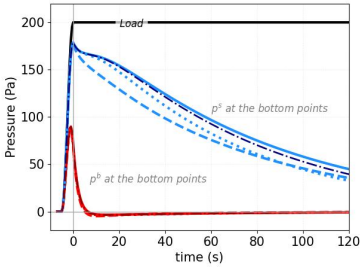

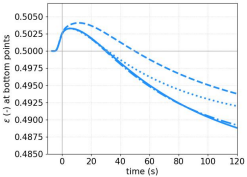

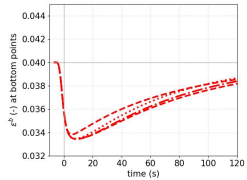

—— $\varepsilon = \varepsilon^l$;
$\varepsilon^l/\varepsilon$ =85%; $\varepsilon^c/\varepsilon$ =15%: - - - $\mu^c = 1\text{Pa s}$; ····· $\mu^c = 5\text{Pa s}$; —·— $\mu^c = 20\text{Pa s}$.

Computational Framework using FEniCSx

- ✔ A **modular** mathematical model,
- ✔ Inclusion of a **vascular** compartment,
- ✔ **Open-Source Framework** with **tutorials, GitHub repos and symposiums**,
- ✔ At short time scales, **cells** behave as a **solid**,

Tutorial article; Tutorial repository; Symposium repository; Package repository.

Computational Framework using FEniCSx

- ✔ A **modular** mathematical model,
- ✔ Inclusion of a **vascular** compartment,
- ✔ **Open-Source Framework** with **tutorials, GitHub repos and symposiums**,
- ✔ At short time scales, **cells** behave as a **solid**,
- ~ Need of clinically relevant data for *in vivo* model **evaluation**,
- ~ Difficulties to identify **boundary conditions** for *in vivo* description. [Wahlsten et al., 2019]
- ~ Increased model **complexity** leads to experimental **limits** $\Longrightarrow$ motivates new **collaborations**.

Computational Framework using FEniCSx

- ✔ A **modular** mathematical model,
- ✔ Inclusion of a **vascular** compartment,
- ✔ **Open-Source Framework** with **tutorials, GitHub repos and symposiums**,
- ✔ At short time scales, **cells** behave as a **solid**,
- ~ Need of clinically relevant data for *in vivo* model **evaluation**,
- ~ Difficulties to identify **boundary conditions** for *in vivo* description. [Wahlsten et al., 2019]
- ~ Increased model **complexity** leads to experimental **limits** $\Longrightarrow$ motivates new **collaborations**.

The mathematical framework has been established. The next step is to evaluate the model from a simple system to a more complex description.

Can we model the biological and mechanical response interplay using a poromechanical approach?

☞ Can a poromechanical model reproduce the time-dependent response of the skin?

Can we model the biological and mechanical response interplay using a poromechanical approach?

Application to an *in vivo* extension test: a single-compartment poromechanical model.

This work is under 2nd review in the *International Journal of Numerical Method in Biomedical Engineering* and has been presented during EPUAP 2024, F2M 2024, Interpore 2024.

femto-st SCIENCES & TECHNOLOGIES

Biphasic model of the skin in traction

Challenge our implementation with a **simple model** (no chemo-mechanical coupling) with ***in vivo*** **experiments**.

[Wahlsten et al., 2019, Sachs et al., 2021]

Experimental data

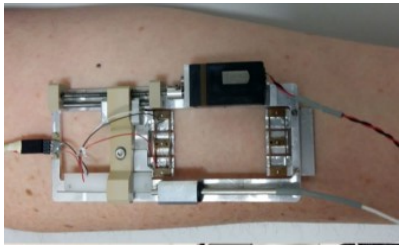

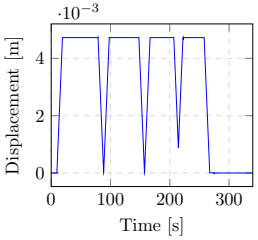

Experimental device [Chambert et al., 2019] and imposed disp.

- *In vivo* upper arm skin of a 22 y-o female,
- 4 load-sustain-unload cycles,
- Imposed displacement, controlled reaction force (RF),
- 1.00 mm s^{-1} controlled speed,
- 9.50 mm maximum displacement.

Model Geometry

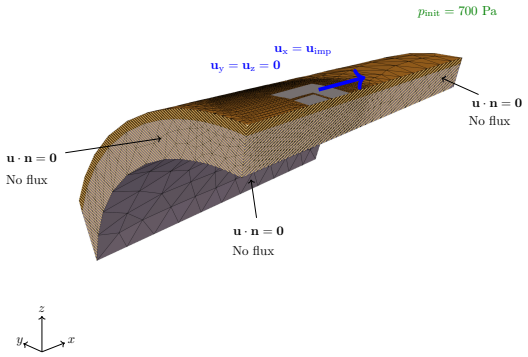

Phase \ Species	ECM	Other structures (glands, hair, etc.)	Cells	Water	Oxygen	Other Species
Solid (s)	✓	✓	✓	✓		✓
Liquid (l)				✓	✓	✓

- Cutis ≈ 2 mm (echography),
- Subcutis ≈ 8 mm [Birkebaek et al., 1998, Mellor et al., 2004],
- Radius = 48 mm [Elouneg, 2023].

Variance-based sensitivity

The model has been implemented in **FEniCSx**. To limit the effect of local minima, only **Young moduli** and **permeabilities** were calibrated. To support this choice, variance-based sensitivity indices have been computed:

- Parameter variation $\delta = \pm 10\%$,
- Error metric: $mean(RF_{ref} - RF_{\delta})|_{t \in [18,\, 50]}$,
- Sensitivity' indices: $S_i = \frac{\theta_i^2}{\sum \theta_i^2}$,
- The parameters accounting for 95% of the variance are considered for the calibration.

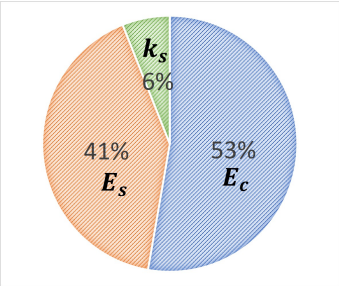

Calibration procedure

A RMSE functional has been introduced:

$$\text{RMSE} = \sqrt{\frac{\sum\limits_{t\in[20,\ 75]} (RF - RF_{\text{theo}})^2 + \sum\limits_{t\in[98,\ 140]} (RF - RF_{\text{theo}})^2}{\text{Number of steps}}} \tag{3}$$

Controlled Random Search algorithm [Kaelo and Ali, 2006] from NLOPT with:

$$[10\text{ kPa},\ 10\text{ kPa},\ 1\times10^{-16}\text{ m}^2,\ 1\times10^{-16}\text{ m}^2] \leq [E_c,\ E_s,\ k_c,\ k_s]$$

$$[500\text{ MPa},\ 500\text{ MPa},\ 1\times10^{-10}\text{ m}^2,\ 1\times10^{-10}\text{ m}^2] \geq$$

Initial population size: $3\times(NN+1)$

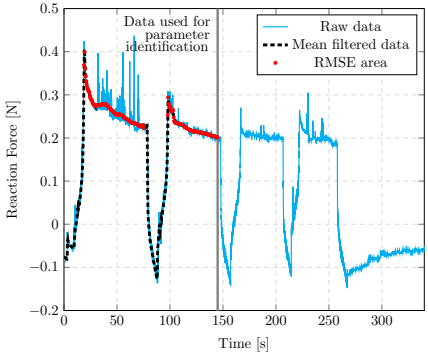

Reaction force / time experimental and filtered curves.

Calibration procedure

Cutis Parameters	Initial Value	Unit
→ Young's modulus (E_c)	1.5×10^5	Pa
Poisson's ratio (ν_c)	0.48	-
→ Intrinsic permeability (k_c)	4×10^{-14}	m^2
Initial Porosity (ε_c^I)	0.2	-
Subcutis Parameters	Value	Unit
→ Young's modulus E_s	1×10^5	Pa
Poisson's ratio (ν_s)	0.3	-
→ Intrinsic permeability (k_s)	3×10^{-13}	m^2
Initial Porosity (ε_s^I)	0.4	-
Fluid phase	Value	Unit
IF viscosity (μ^I)	5×10^{-3}	Pa s

Fixed parameters

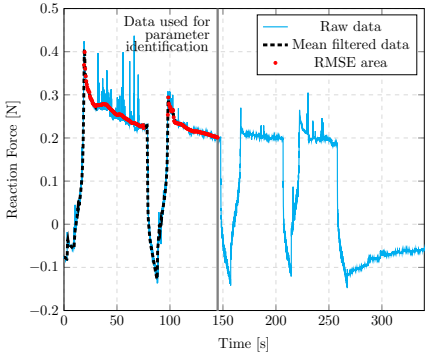

Reaction force / time experimental and filtered curves.

Results

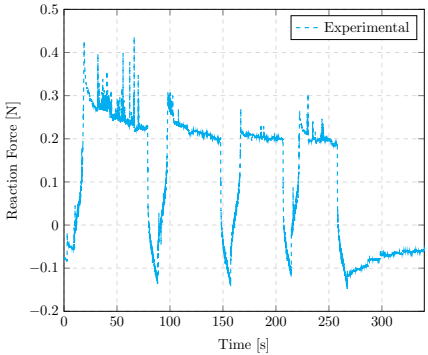
Experimental
Reaction Force [N]
Time [s]
0.5
0.4
0.3
0.2
0.1
0
−0.1
−0.2
0
50
100
150
200
250
300

Results

- Good agreement between the experiment and the model: RMSE$= 8.8 \times 10^{-3}$ N $\approx 2\% RF_{peak}$,

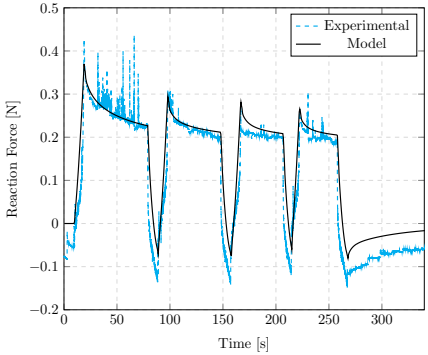

Results

- Good agreement between the experiment and the model: RMSE$= 8.8 \times 10^{-3}$ N $\approx 2\% RF_{peak}$,
- The final reflux is captured,

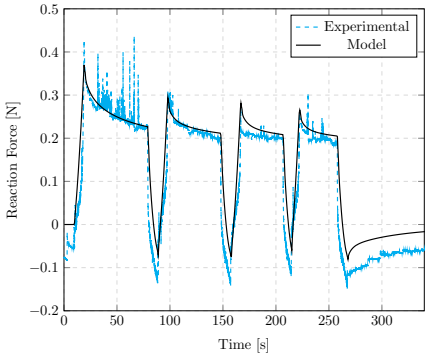

Results

- Good agreement between the experiment and the model: RMSE$= 8.8 \times 10^{-3}$ N $\approx 2\% RF_{peak}$,
- The final reflux is captured,
- Material parameters consistent with the literature.

Cutis Parameter	Value	Unit
Young modulus (E_c)	684×10^3	Pa
Intrinsic permeability (k_c)	9.43×10^{-15}	m^2
Subcutis Parameter	Value	Unit
Young modulus (E_s)	47.8×10^3	Pa
Intrinsic permeability (k_s)	5.03×10^{-13}	m^2

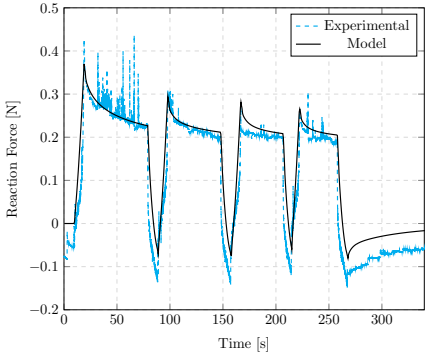

Physical insights

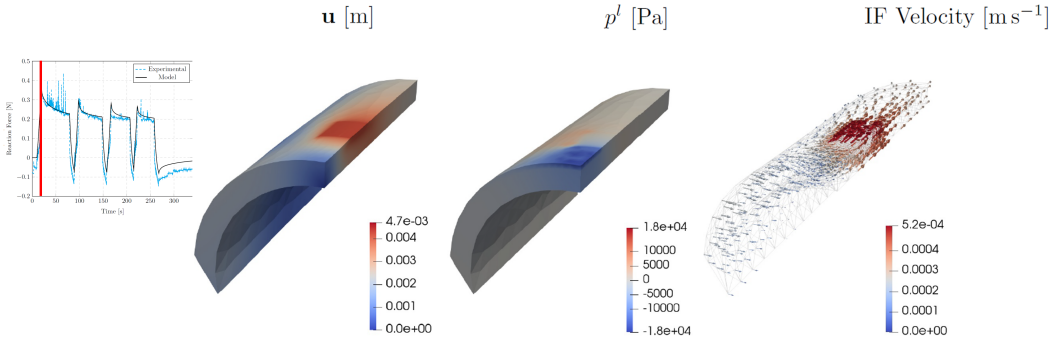

When stretching the skin, the fluid underneath the patch slowly follows the patch movements and the neighbouring fluid is drawn in the pores.

Physical insights

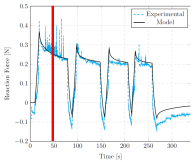

$\mathbf{u}$ [m]

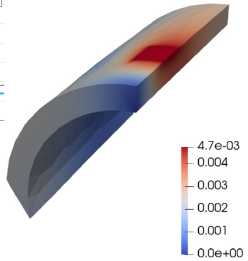

p^l [Pa]

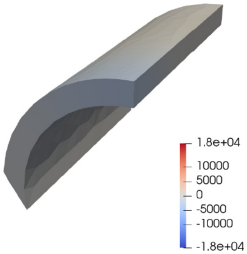

IF Velocity [$\mathrm{m\,s^{-1}}$]

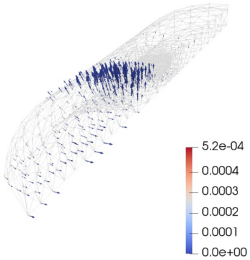

During a sustained phase, an equilibrium phase is reached and the fluid moves from the subcutis to the cutis.

Physical insights

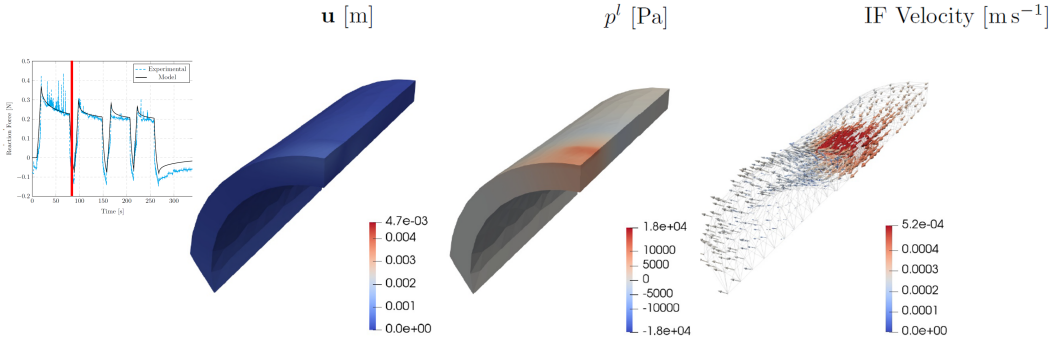

During a release phase, the fluid is expelled from the deformed region to be replaced by the one underneath the patch.

Physical insights

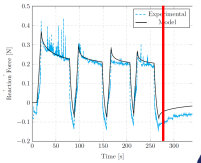

$\mathbf{u}$ [m]

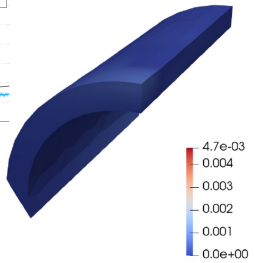

p^l [Pa]

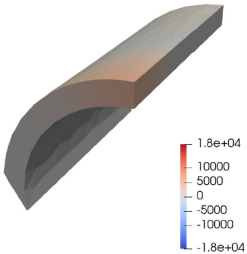

IF Velocity [$\mathrm{m\,s^{-1}}$]

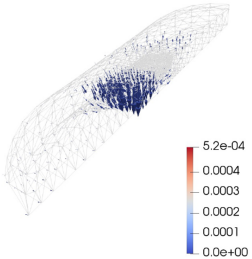

During the last stage, the initial state is reached again and a movement of fluid from the cutis to the subcutis is expected.

Discussion

- ✔ **Good agreement** between the *in vivo* experimental and the model reaction forces,
- ✔ The calibrated parameters **align with previously reported values**, confirming that the subcutis is softer than the cutis [Sachs et al., 2021],
- ✔ Valuable insights are identified in **the understanding of the time dependent response**,
- ✔ **Alternative** to empirical visco-elastic models,

Discussion

- ✔ **Good agreement** between the *in vivo* experimental and the model reaction forces,
- ✔ The calibrated parameters **align with previously reported values**, confirming that the subcutis is softer than the cutis [Sachs et al., 2021],
- ✔ Valuable insights are identified in **the understanding of the time dependent response**,
- ✔ **Alternative** to empirical visco-elastic models,
- ~ **Noisy** data (sensors initially developed for keloids),
- ~ A single experiment on a single subject was accessible $\Longrightarrow$ **further experiments** with different loading conditions and regions are required,
- ~ Difficult to **distinguish between viscoelastic and poroelastic dissipation** when only limited boundary condition information is known.

Discussion

- ✔ **Good agreement** between the *in vivo* experimental and the model reaction forces,
- ✔ The calibrated parameters **align with previously reported values**, confirming that the subcutis is softer than the cutis [Sachs et al., 2021],
- ✔ Valuable insights are identified in **the understanding of the time dependent response**,
- ✔ **Alternative** to empirical visco-elastic models,
- ~ **Noisy** data (sensors initially developed for keloids),
- ~ A single experiment on a single subject was accessible $\Longrightarrow$ **further experiments** with different loading conditions and regions are required,
- ~ Difficult to **distinguish between viscoelastic and poroelastic dissipation** when only limited boundary condition information is known.

We evaluated the simplest model implementation with regard to experimental data. The next step is to assess the **feasibility** of using our **modular approach** for **perfused tissue**.

Can we model the biological and mechanical response interplay using a poromechanical approach?

☞ How can we evaluate the poromechanical model with the vascular system?

Can we model the biological and mechanical response interplay using a poromechanical approach?

Application to an *in vivo* indentation test: a two-compartment poromechanical model.

This work is accepted in *International Journal of Numerical Method in Biomedical Engineering*

Experimental data: laser doppler flowmetry (LDF)

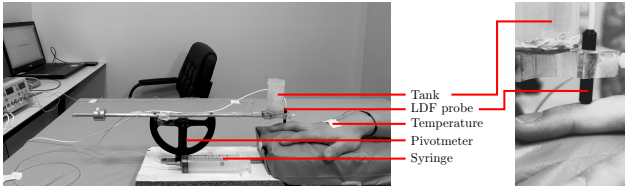

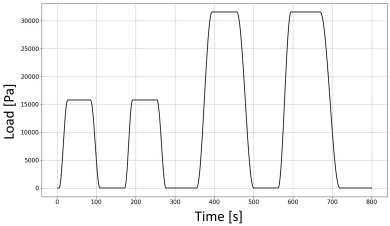

- N=11: 6 M & 5 F (25±2 y-o),
- 4 × (4 load-sustain-unload cycles), 2 consecutive days
- Imposed load, controlled flow, monitored temperature,
- 1.00 mL s^{-1} controlled speed,
- 40.00 mL maximum load.

Ethical approval N°2023-A00418-37

Raw experimental results

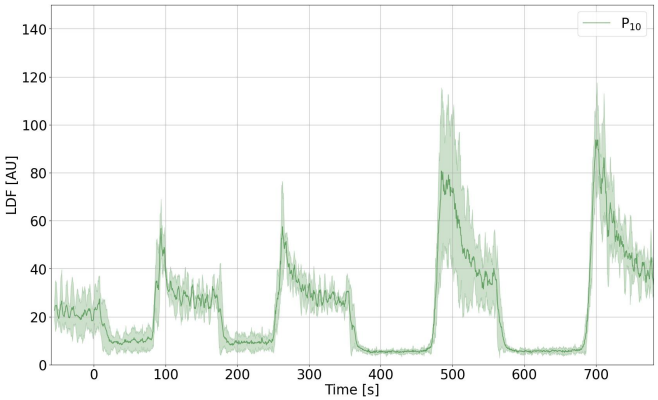

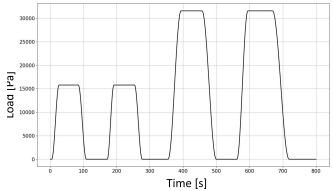

- LDF = Blood cells concentration $\times$ blood velocity
- Load $\Longrightarrow$ ischaemia; release $\Longrightarrow$ reactive hyperemia.

Raw experimental results

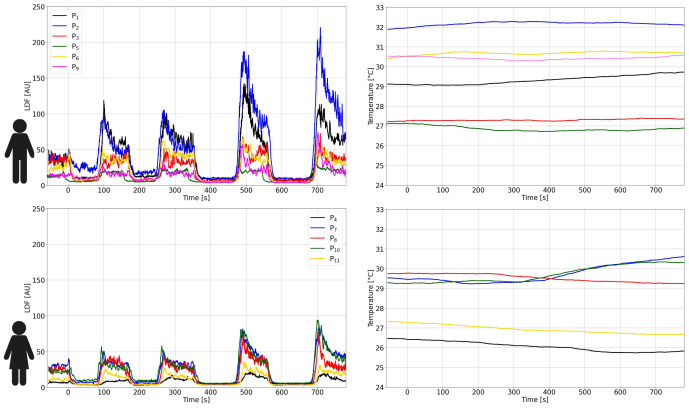

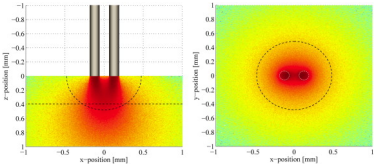

[Fredriksson et al., 2009]

$$LDF = \int_{\Omega_{LDF}} ||\varepsilon^b(v^b - v^s)|| \, \mathrm{d}\Omega$$

Variation with respect to the basal blood flow

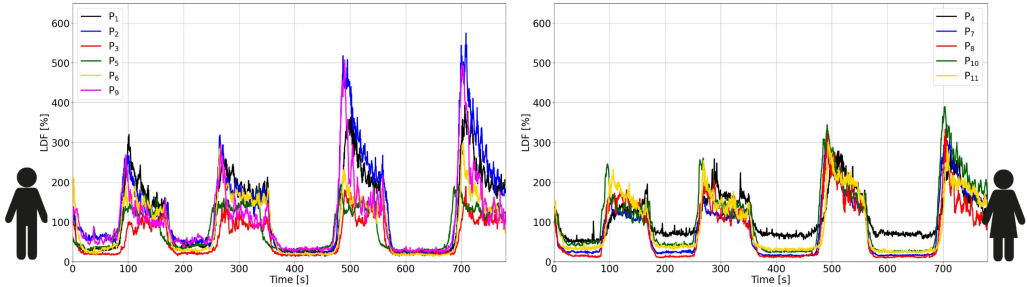

Men (left) Women (right)

$$LDF\,[\%] = \frac{\int_{\Omega_{LDF}} \sqrt{\varepsilon^b(v^b - v^s) \cdot \varepsilon^b(v^b - v^s)}\mathrm{d}\Omega}{LDF_0} \tag{3}$$

Model description

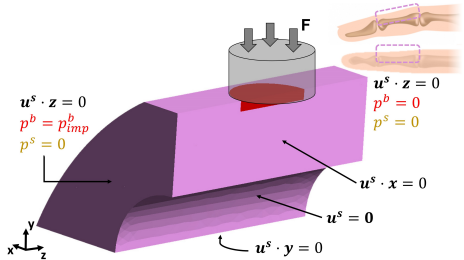

Phase \ Species	ECM	Other structures (glands, hair, etc.)	Cells	Water	Oxygen	Other Species
Solid (s)	✓	✓	✓	✓		✓
Liquid (l)				✓	✓	✓
Vascular (blood) (b)				✓	✓	✓

Parameter	Initial	Minimal	Maximal
Young Modulus (E)	2.00×10^5Pa	5.00×10^4Pa	1.00×10^6Pa
Hydraulic permeability IF (L^l)	1×10^{-14}m^2 Pa^{-1} s^{-1}	1×10^{-15}m^2 Pa^{-1} s^{-1}	1×10^{-13}m^2 Pa^{-1} s^{-1}
Hydraulic permeability Blood (L^b)	1×10^{-9}m^2 Pa^{-1} s^{-1}	1×10^{-10}m^2 Pa^{-1} s^{-1}	1×10^{-8}m^2 Pa^{-1} s^{-1}
α	3	2	6
Vessel Compressibility (K)	1000	500	5000

Variance-based sensitivity analysis

The first and second-order analysis give the variance-based sensitivity indices:

$$S_i = \frac{\theta_i^2}{\sum_i \theta_i^2} \quad \text{and} \quad S_i = \frac{\theta_i^2}{\sum_i \theta_i^2 + \sum_{ij,i>j} \theta_{ij}^2} \quad ; \quad S_{ij} = \frac{\theta_{ij}^2}{\sum_i \theta_i^2 + \sum_{ij,i>j} \theta_{ij}^2} \qquad (4)$$

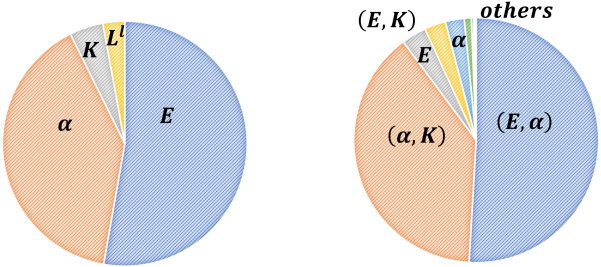

Model response using FEniCSx

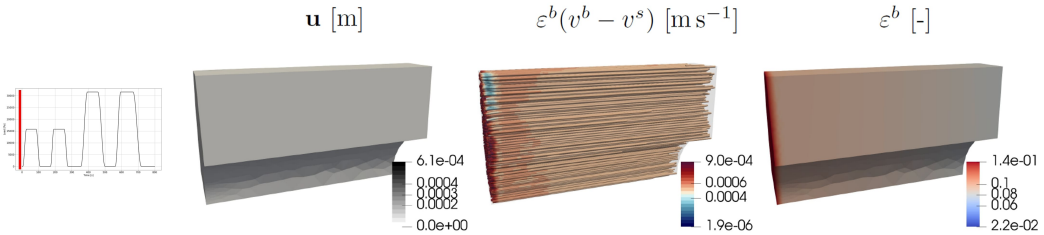

Initially, the BCs allow for a basal blood flow.

Model response using FEniCSx

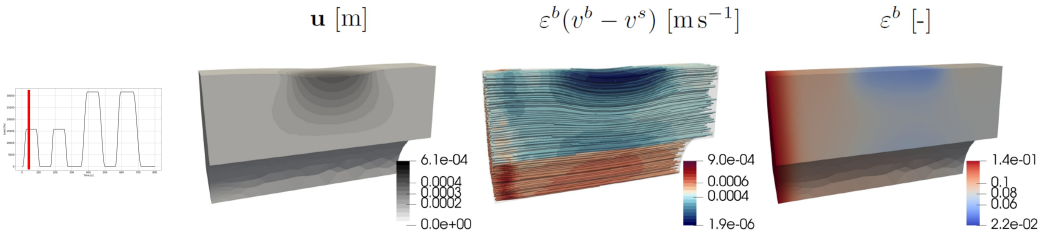

When indenting the skin, the flow is locally reduced and the vascular porosity decreases.

Model response using FEniCSx

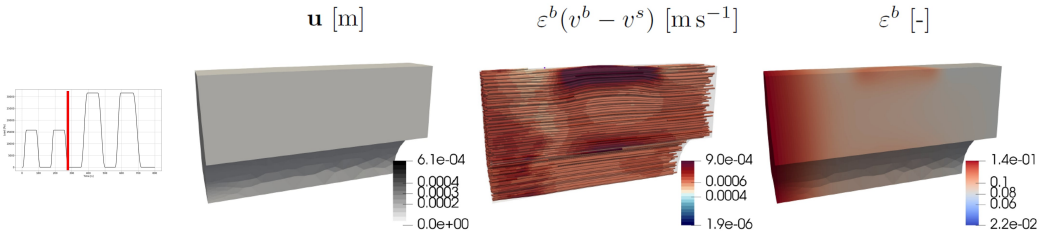

Vasodilation is observed with an increase blood flow during and directly after the release of the load

Model response using FEniCSx

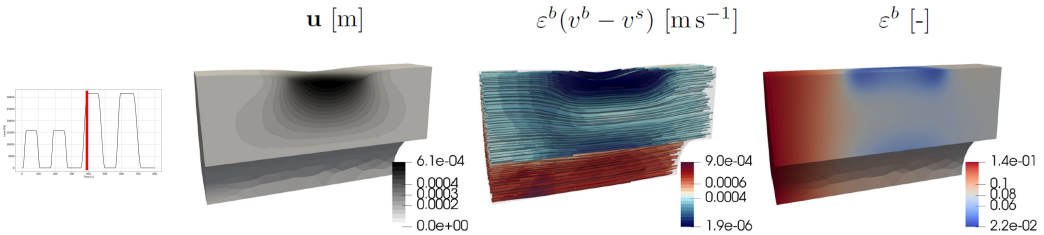

A larger area of reduced flow is observed for higher load magnitude.

Model response using FEniCSx

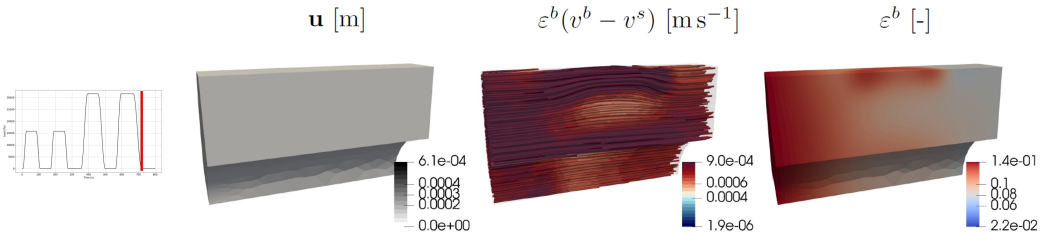

PORH is more intense when a more intensive load is released.

Evaluation of the model

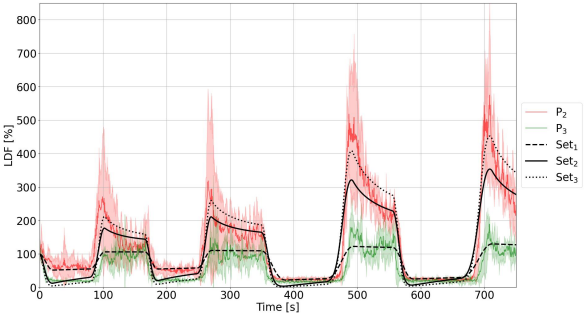

Set	E [Pa]	L^l [m^2 Pa^{-1} s^{-1}]	L^b [m^2 Pa^{-1} s^{-1}]	α [-]	K [Pa]
Set_1	2×10^5	10^{-14}	10^{-9}	3	10^3
Set_2	2×10^5	10^{-13}	10^{-9}	5	10^3
Set_3	8×10^4	10^{-13}	10^{-9}	6	10^3

Discussion

- ✔ **Experimental campaign** carried out,
- ✔ **Ischaemia** and **Post Occlusive Hyperaemia** (PORH) were observed,
- ✔ Relative Ischaemia and PORH are **comparable between genders**,
- ✔ **Mechanics** play a role in **PORH**,
- ✔ **Model capacity** to reproduce ischaemia and PORH,
- ✔ Suitable for **parallel computation**,
- ✔ Allows for a future introduction of **biological exchanges**,

Discussion

- ✔ **Experimental campaign** carried out,
- ✔ **Ischaemia** and **Post Occlusive Hyperaemia** (PORH) were observed,
- ✔ Relative Ischaemia and PORH are **comparable between genders**,
- ✔ **Mechanics** play a role in **PORH**,
- ✔ **Model capacity** to reproduce ischaemia and PORH,
- ✔ Suitable for **parallel computation**,
- ✔ Allows for a future introduction of **biological exchanges**,
- ~ More accurate control of the **BCs** is required for a more **complete evaluation**,
- ~ There is **not a clear consensus** on material parameters and BCs in the literature yet,
- ~ Future work should complete the experimental campaign and assess **subject-specific calibration**.

Develop and evaluate a poromechanical model that couples mechanical behaviour and micro-circulation.

Challenges

- ☞ How can we introduce the vascular system to a poromechanical model for the skin?
- ☞ How can we evaluate the poromechanical model with the vascular system?

Conclusion

- ✔ **Hierarchical and Modular** mathematical framework (underlying physics),
- ✔ **Vascular compartment** introduction $\Longrightarrow$ towards biological processes,
- ✔ **Ischaemia** and **PORH** were obtained with **mechanics** only,
- ✔ **Open-source** implementation, with a **special care on reproductibility**,
- ✔ The **complexity** of the model motivated **new** collaboration for **experimental** evaluation based on:
  - — existing experimental data,
  - — **newly acquired data** as part of this PhD work
- ✔ **Transferable**: plantar foot, brain, tissue engineering, drug delivery,

Conclusion

- Future work will focus in enhancing the **boundary condition** identification for subject specific analysis,
- The *in silico* evaluation of some mechanical properties could tighten the **uncertainty sources**,
- Biological integration should be compared to **experimental campaigns** (M Lacour & C Cornillon PhDs),
- For pressure ulcers prevention, **damage** and **remodelling** should be introduced,
- One could think in **Machine Learning** integration to reduce computational times, especially in the realm of subject specific analysis and **clinical integration**.

Acknowledgments

This research was funded in whole, or in part, by the Luxembourg National Research Fund (FNR), grant reference No. 17013182. I would like to thank my supervisors, the participants to the experiment, as well as each individual that contributed to this PhD outcomes.

Thank you!

Do you have any questions?

Appendix: Papillary plexus

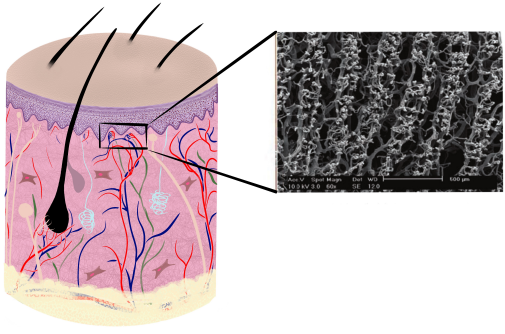

Unpublished data, courtesy of Fromy et al.

Appendix: Langer lines

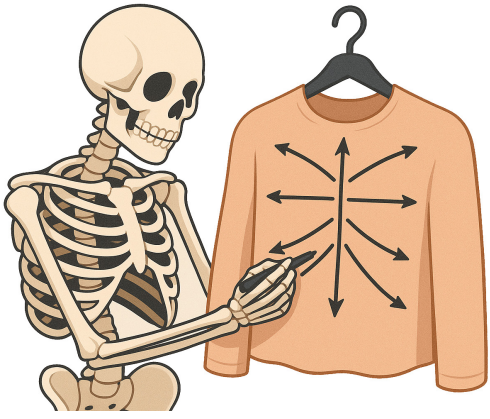

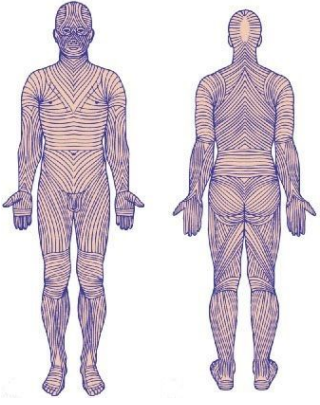

Carmichael SW.The tangled web of Langer's lines.Clin Anat. 2013

Appendix: Boundary conditions

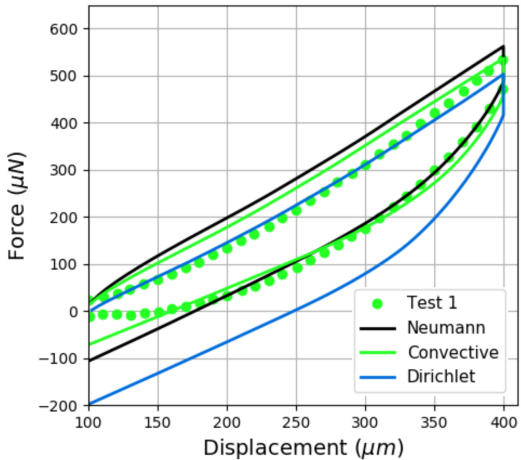

[Urcun et al., 2022]

Appendix: drug delivery

Porous media mechanics allows the introduction of drugs too.
[de Lucio et al., 2023, de Lucio et al., 2024]

Scenarios

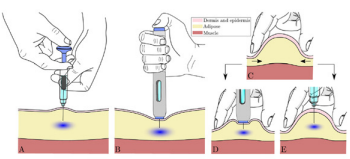

Simulations

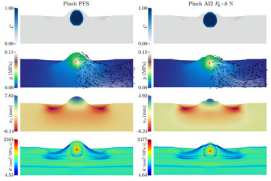

Ex vivo animal evaluation

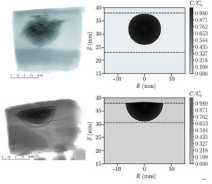

Appendix: Continuity equations

We apply the **continuity equation** to each of the phases:

$$\frac{\mathrm{D}^s \rho^s \varepsilon^s}{\mathrm{Dt}} + \rho^s \varepsilon^s \nabla \cdot \mathbf{v}^s = 0 \text{ on } \Omega, \quad (5)$$

$$\underbrace{\frac{\mathrm{D}^s \rho^\alpha \varepsilon^\alpha}{\mathrm{Dt}}}_{\text{Accumulation rate}} + \underbrace{\rho^\alpha \varepsilon^\alpha \nabla \cdot \mathbf{v}^s}_{\text{ECM deformation}} + \underbrace{\nabla \cdot (\rho^\alpha \varepsilon^\alpha (\mathbf{v}^\alpha - \mathbf{v}^s))}_{\text{Infiltration}} = 0 \text{ on } \Omega, \ \alpha \in [l, c, b], \quad (6)$$

Implemented and benchmarked in FEniCSx [Lavigne et al., 2023]; Unkowns / Material Parameters;

The developments to get the coupled continuity equation are provided in [Lavigne et al., 2023].

Appendix: Remark: Introducing the oxygen biochemistry.

Consider the **exchange of oxygen** between the blood compartment and cells in the extravascular space through the interstitial fluid.

$$\underbrace{\frac{\mathrm{D}^s}{\mathrm{D}t}(\varepsilon^l \rho^l \omega^{O2,l})}_{\text{Accumulation rate}} + \underbrace{\nabla \cdot (\varepsilon^l \rho^l \omega^{O2,l}(\mathbf{v}^l - \mathbf{v}^s))}_{\text{Convection}} + \underbrace{\nabla \cdot (\varepsilon^l \rho^l \omega^{O2,l} \mathbf{u}^{O2,l})}_{\textit{Diffusion}} + \underbrace{\varepsilon^l \rho^l \omega^{O2,l} \nabla \cdot \mathbf{v}^s}_{\text{ECM deformation}} = \underbrace{\overset{O2,b \to O2,l}{M}}_{\text{Blood to IF transport}} - \underbrace{\overset{O2,l \to O2,c}{M}}_{\text{O2 consumption from the cells}} \tag{7}$$

(Extension of the model proposed by [Sciumè, 2021]).

Appendix: Momentum Conservation

We apply the **momentum conservation** to the total stress tensor:

$$\nabla \cdot \mathbf{t}^{\mathrm{tot}} + \mathbf{b} = 0 \text{ on } \Omega, \tag{8}$$

Stress tensor solid phase:

$$\mathbf{t}^s = \tau^s - p^s \mathbf{1}$$

$\approx$ Effective solid phase stress tensor

Solid phase pressure

Stress for fluid phases:

$$\mathbf{t}^f = -p^f \mathbf{1}$$

Pressure in the fluid phase (positive if the fluid is in compression)

$$\mathbf{t}^{\mathrm{tot}} = \sum_{\alpha=s,b,c,l} \varepsilon^\alpha \mathbf{t}^\alpha = \varepsilon^s \tau^s - \varepsilon^s p^s \mathbf{1} - \sum_f \varepsilon^f p^f \mathbf{1} \tag{9}$$

Appendix: Momentum conservation

For the fluid phases, the momentum conservation reads:

$$-\frac{\mathbf{K}^f}{\mu^f}\nabla p^f = \varepsilon^f\left(\mathbf{v}^f - \mathbf{v}^s\right),\ (f = l, c, b) \tag{10}$$

Appendix: Variance-based Sensitivity Tables

The model has been implemented in FEniCSx. To limit the effect of local minima, only the **Young moduli** and **permeabilities** were calibrated. To support this choice, the Sobol' indices have been computed:

- Parameter variation $\delta = \pm 10\%$,
- Error metric: $mean(RF_{ref} - RF_{\delta})|_{t \in [18,\, 50]}$,
- Sensitivity' indices: $S_i = \frac{\theta_i^2}{\sum \theta_i^2}$,
- The parameters accounting for 90% of the variance are considered for the calibration.

	θ_i	S_i
E_c	28.7	5.27×10^{-1}
E_s	25.4	4.12×10^{-1}
ε_c	-2.44×10^{-5}	3.80×10^{-13}
ε_s	-2.06×10^{-4}	2.71×10^{-11}
k_c	-1.6×10^{-1}	1.64×10^{-5}
k_s	-9.71	6.02×10^{-2}
p_{init}	-1.09×10^{-4}	7.63×10^{-12}

Appendix: Variance-based Sensitivity Tables

Parameter	θ_i or θ_{ij} [IU]	S_i or S_{ij} [%]
Young Modulus (E)	2.00×10^{-1}	52.78
α	-1.74×10^{-1}	39.87
Vessel Compressibility (K)	5.83×10^{-2}	4.46
Hydraulic permeability ISF (L^I)	4.68×10^{-2}	2.88
Hydraulic permeability Blood (L_0^b)	-2.07×10^{-3}	5.64×10^{-3}

Appendix: Variance-based Sensitivity Tables

Parameter	θ_i or θ_{ij} [IU]	S_i or S_{ij} [%]
(E, α)	-7.90×10^{-1}	50.9
(α, K)	-6.90×10^{-1}	38.9
Young Modulus (E)	2.00×10^{-1}	3.28
(E, K)	1.86×10^{-1}	2.81
α	-1.74×10^{-1}	2.48
(E, L^l)	1.08×10^{-1}	0.94
Vessel Compressibility (K)	5.83×10^{-2}	0.27
(L_0^b, α)	-4.76×10^{-2}	0.19
Hydraulic permeability ISF (L^l)	4.68×10^{-2}	0.17
(L_0^b, K)	-8.94×10^{-3}	6.53×10^{-3}
(L^l, L_0^b)	-5.80×10^{-3}	2.75×10^{-3}
(L^l, K)	3.83×10^{-3}	1.19×10^{-3}
(L^l, α)	2.22×10^{-3}	4.03×10^{-4}
Hydraulic permeability Blood (L_0^b)	-2.07×10^{-3}	3.50×10^{-4}
(E, L_0^b)	-1.19×10^{-3}	1.16×10^{-4}

Appendix: Porous parameters table

Reference	Porosity (-)	Viscosity (cPa s)	Intrinsic Permeability (m^2)	Hydraulic permeability ($m^2\,Pa^{-1}\,s^{-1}$)
[Wiig and Swartz, 2012]	$0.2 - 0.5$	*1*	*1×10^{-9}; 1×10^{-7}*	*1×10^{-7}; 1×10^{-5}*
[Humphrey and O'Rourke, 2015]	N-S	1.2; 3.5	N-S	N-S
[Hoskins et al., 2017]	N-S	0.28; 1.5	N-S	N-S
[Oftadeh et al., 2018]	N-S	*1*	*$(1.47\pm0.23)\times10^{-15}$*	$(1.47 \pm 0.23) \times 10^{-13}$
[Samant and Prausnitz, 2018]	0.24 ± 0.06	N-S	N-S	N-S
[Wahlsten et al., 2019]	0.7	*1*	*5×10^{-15}*	5×10^{-13}
[Sowinski et al., 2021]	N-S	0.07-6.77	N-S	N-S
[Leng et al., 2021]	0.1	1	9.8×10^{-14}; 9.8×10^{-12}	*9.8×10^{-12}; 9.8×10^{-10}*
[Han et al., 2023]	0.01	*1*	1×10^{-15}; 1×10^{-13}	*1×10^{-13}; 1×10^{-11}*
[Torres-Terán et al., 2023]	N-S	0.1; 0.15	N-S	N-S
[Oftadeh et al., 2023]	N-S	*1*	*$0.5\text{-}2\times10^{-16}$*	$0.5\text{-}2\times10^{-14}$

Appendix: LDF Statistics and values (M)

Normality tests were conducted to assess the distribution of the data. As the variables were not normally distributed, nonparametric tests were used. A Wilcoxon rank-sum test was performed ($6 \times 4 = 24$ samples).

	Median	IQR	T-statistic	p-value
Temperature [°C]	29.5	2.8		
Basal flow [AU]	24.7	19.9		
LDF Isch. 20mL [AU]	8	5.5	36.3	1.30E-08
LDF Isch. 20mL [%]	38.5	25.8	25.9	2.30E-06
LDF Isch. 40mL [AU]	5.6	3.2	5.1	0.06
LDF Isch. 40mL [%]	22.8	9.4	57.3	3.50E-13
LDF Hyp. 20mL [AU]	66.7	76.1	26	2.20E-06
LDF Hyp. 20mL [%]	251.8	129.5	23.5	7.90E-06
LDF Hyp. 40mL [AU]	94.1	89.3	5.8	6.00E-02
LDF Hyp. 40mL [%]	353	270.5	14.9	5.70E-04

Appendix: LDF Statistics and values (F)

Normality tests were conducted to assess the distribution of the data. As the variables were not normally distributed, nonparametric tests were used. A Wilcoxon rank-sum test was performed ($5 \times 4 = 20$ samples).

	Median	IQR	T-statistic	p-value
Temperature [°C]	27.8	2.6		
Basal flow [AU]	16.6	17.3		
LDF Isch. 20mL [AU]	4.9	3.8	10.9	4.00E-03
LDF Isch. 20mL [%]	32.8	24.2	17.6	1.50E-04
LDF Isch. 40mL [AU]	4.3	1.9	0.9	0.6
LDF Isch. 40mL [%]	24.3	17.9	15.8	3.70E-04
LDF Hyp. 20mL [AU]	45.9	26.1	5.3	7.00E-02
LDF Hyp. 20mL [%]	255.6	113.2	2.4	3.00E-01
LDF Hyp. 40mL [AU]	60.3	58.5	7.3	3.00E-02
LDF Hyp. 40mL [%]	336.4	144.6	2.6	3.00E-01

Appendix: LDF Statistics and values (M-F)

Independent Wilcoxon rank tests null hypothesis: two sets of measurements are drawn from the same distribution. The results showed **significant differences in terms of raw AU signals** but did **not** show significant differences when looking to the **relative evolution to the basal blood flow** (p-values $\gg$ ($\alpha = 0.05$)). These results further suggest that **temperature primarily affects basal skin blood flow** rather than the microvascular response to load-induced ischaemia and subsequent hyperaemia.

	T-statistic	p-value
LDF Isch. 20mL [AU]	4.13	3.60E-05
LDF Isch. 20mL [%]	0.96	0.34
LDF Isch. 40mL [AU]	3.76	1.70E-04
LDF Isch. 40mL [%]	0.41	0.69
LDF Hyp. 20mL [AU]	3.41	6.50E-04
LDF Hyp. 20mL [%]	0.69	0.49
LDF Hyp. 40mL [AU]	3.05	2.30E-03
LDF Hyp. 40mL [%]	0.46	0.64

Appendix: What about the future

Imaging in biomechanics

Meryem Abbad Andaloussi[a,*], Marie Lontsie Zanmene[a], Thomas Lavigne[a,b,c], Vincent Lubrano[d], Stephane Urcun[a], François Hild[e], Stéphane Bordas[a]

Numerical domain preparation:

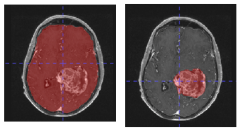

Brain + tumor masks (.nii)/(.dcm)
ITK snap

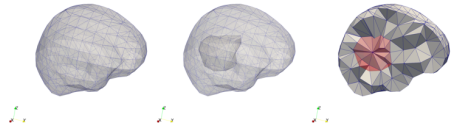

3D surface (brain + tumor) (.stl)
Meshlab

3D volume (brain + tumor) (.stl)
GMSH + paraview

Numerical domain on Image

DVC

Residuals

Full field displacement

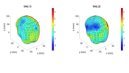

Displacement on Slices of interest

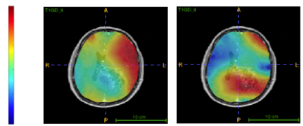

U_x (mm)

U_y (mm)

Appendix: Towards *in silico* evaluation of the permeability

The generation of synthetic geometries is based on the Open Source Crystallographic Software **Neper** and the Open Source Mesh Python Libraries **Pymesh**. The mesh is then transformed to the particle space using **stl2voxel**.

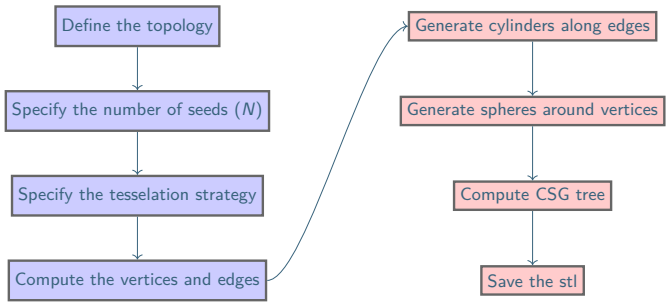

Appendix: Particle Method for fluid dynamics

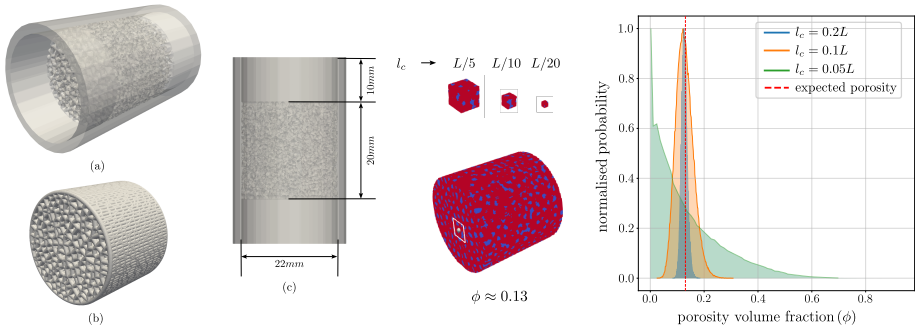

Sample computational domain for **permeability evaluation**, computation of the characteristic length.

Particle Method for fluid dynamics

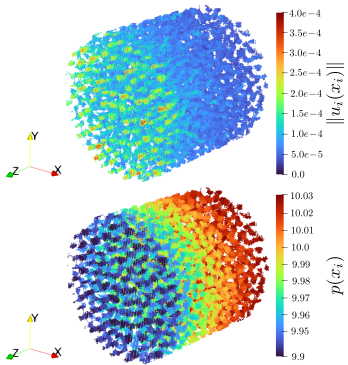

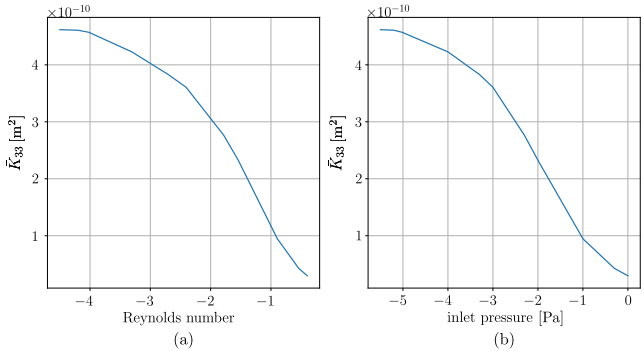

Example output fields R.O.I: velocity and pressure distribution with the resulting permeability estimation: $\bar{K}_{33} \approx -\mu\phi \left(\frac{\Delta p}{\Delta z}\right)^{-1} \langle u_3 \rangle_{,}$.

Appendix: Possible Experimental campaign

Designed **experimental bench and experimental set-up** at Laboratoire de Mécanique Paris-Saclay.

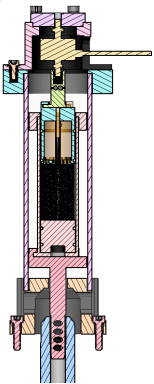

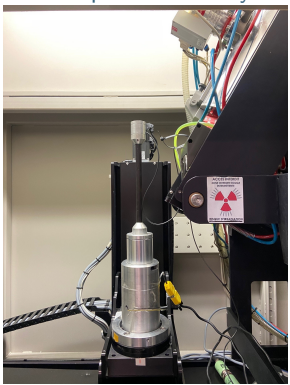

References

Agache, P. G., Monneur, C., Leveque, J. L., and Rigal, J. D. (1980).
Mechanical properties and young's modulus of human skin in vivo.
Archives of Dermatological Research, 269(3):221–232.

Annaidh, A. N., Bruyère, K., Destrade, M., Gilchrist, M. D., and Otténio, M. (2012).
Characterization of the anisotropic mechanical properties of excised human skin.
Journal of the Mechanical Behavior of Biomedical Materials, 5(1):139–148.

Anthony, D., Parboteeah, S., Saleh, M., and Papanikolaou, P. (2008).
Norton, waterlow and braden scores: a review of the literature and a comparison between the scores and clinical judgement.
Journal of Clinical Nursing, 17(5):646–653.

Birkebaek, N., Johansen, A., and Solvig, J. (1998).
Cutis/subcutis thickness at insulin injection sites and localization of simulated insulin boluses in children with type 1 diabetes mellitus: need for individualization of injection technique?
Diabetic Medicine, 15(11):965–971.

Bouten, C. V., Oomens, C. W., Baaijens, F. P., and Bader, D. L. (2003).
The etiology of pressure ulcers: Skin deep or muscle bound?
Archives of Physical Medicine and Rehabilitation, 84(4):616–619.

Boyer, G., Zahouani, H., Bot, A. L., and Laquieze, L. (2007).
In vivo characterization of viscoelastic properties of human skin using dynamic micro-indentation.
In *2007 29th Annual International Conference of the IEEE Engineering in Medicine and Biology Society*. IEEE.

References

Budday, S., Ovaert, T. C., Holzapfel, G. A., Steinmann, P., and Kuhl, E. (2019).
Fifty shades of brain: A review on the mechanical testing and modeling of brain tissue.
Archives of Computational Methods in Engineering, 27(4):1187–1230.

Bulle, R. (2022).
A posteriori error estimation for finite element approximations of fractional Laplacian problems and applications to poro-elasticity.
Theses, Université Bourgogne Franche-Comté ; Université du Luxembourg.

Burns, T., Breathnach, S. M., Cox, N. H., and Griffiths, C., editors (2010).
Rook's textbook of dermatology.
Wiley-Blackwell, Chichester, England, 8 edition.

Carrasco-Mantis, A., Randelovic, T., Castro-Abril, H., Ochoa, I., Doblaré, M., and Sanz-Herrera, J. A. (2023).
A mechanobiological model for tumor spheroid evolution with application to glioblastoma: A continuum multiphysics approach.
Computers in Biology and Medicine, 159:106897.

Ceelen, K., Stekelenburg, A., Loerakker, S., Strijkers, G., Bader, D., Nicolay, K., Baaijens, F., and Oomens, C. (2008).
Compression-induced damage and internal tissue strains are related.
Journal of Biomechanics, 41(16):3399–3404.

Chambert, J., Lihoreau, T., Joly, S., Chatelain, B., Sandoz, P., Humbert, P., Jacquet, E., and Rolin, G. (2019).
Multimodal investigation of a keloid scar by combining mechanical tests in vivo with diverse imaging techniques.
Journal of the Mechanical Behavior of Biomedical Materials, 99:206–215.

References

Coleman, S., Gorecki, C., Nelson, E. A., Closs, S. J., Defloor, T., Halfens, R., Farrin, A., Brown, J., Schoonhoven, L., and Nixon, J. (2013).
Patient risk factors for pressure ulcer development: Systematic review.
International Journal of Nursing Studies, 50(7):974–1003.

Coleman, S., Nixon, J., Keen, J., Wilson, L., McGinnis, E., Dealey, C., Stubbs, N., Farrin, A., Dowding, D., Schols, J. M., Cuddigan, J., Berlowitz, D., Jude, E., Vowden, P., Schoonhoven, L., Bader, D. L., Gefen, A., Oomens, C. W., and Nelson, E. A. (2014).
A new pressure ulcer conceptual framework.
Journal of Advanced Nursing, 70(10):2222–2234.

Connesson, N., Briot, N., Rohan, P. Y., Barraud, P. A., Elahi, S. A., and Payan, Y. (2023).
Bilayer stiffness identification of soft tissues by suction.
Experimental Mechanics, 63(4):715–742.

de Lucio, M., Leng, Y., Hans, A., Bilionis, I., Brindise, M., Ardekani, A. M., Vlachos, P. P., and Gomez, H. (2023).
Modeling large-volume subcutaneous injection of monoclonal antibodies with anisotropic porohyperelastic models and data-driven tissue layer geometries.
Journal of the Mechanical Behavior of Biomedical Materials, 138:105602.

de Lucio, M., Leng, Y., Wang, H., Vlachos, P. P., and Gomez, H. (2024).
Modeling drug transport and absorption in subcutaneous injection of monoclonal antibodies: Impact of tissue deformation, devices, and physiology.
International Journal of Pharmaceutics, 661:124446.

References

Demarré, L., Lancker, A. V., Hecke, A. V., Verhaeghe, S., Grypdonck, M., Lemey, J., Annemans, L., and Beeckman, D. (2015).
The cost of prevention and treatment of pressure ulcers: A systematic review.
International Journal of Nursing Studies, 52(11):1754–1774.

Diridollou, S., Patat, F., Gens, F., Vaillant, L., Black, D., Lagarde, J. M., Gall, Y., and Berson, M. (2000).
In vivo model of the mechanical properties of the human skin under suction.
Skin Research and Technology, 6(4):214–221.

Doll, S. and Schweizerhof, K. (2000).
On the development of volumetric strain energy functions.
Journal of Applied Mechanics, 67(1):17–21.

Ehlers, W. and Markert, B. (2001).
A linear viscoelastic biphasic model for soft tissues based on the theory of porous media.
Journal of Biomechanical Engineering, 123(5):418–424.

Ehret, A. E., Bircher, K., Stracuzzi, A., Marina, V., Zündel, M., and Mazza, E. (2017).
Inverse poroelasticity as a fundamental mechanism in biomechanics and mechanobiology.
Nature Communications, 8(1).

Elleuch, K., Elleuch, R., and Zahouani, H. (2006).
Comparison of elastic and tactile behavior of human skin and elastomeric materials through tribological tests.
Polymer Engineering & Science, 46(12):1715–1720.

References

Elouneg, A. (2023).
In vivo mechanical characterization of soft tissues : application to human skin and keloid.
Theses, Université Bourgogne Franche-Comté ; Université du Luxembourg.

Elouneg, A., Chambert, J., Lejeune, A., Lucot, Q., Jacquet, E., and Bordas, S. (2023).
Anisotropic mechanical characterization of human skin by in vivo multi-axial ring suction test.
Journal of the Mechanical Behavior of Biomedical Materials, 141:105779.

Escoffier, C., de Rigal, J., Rochefort, A., Vasselet, R., Léve^que, J.-L., and Agache, P. G. (1989).
Age-related mechanical properties of human skin: An in vivo study.
Journal of Investigative Dermatology, 93(3):353–357.

Fredriksson, I., Larsson, M., and Strömberg, T. (2009).
Measurement depth and volume in laser doppler flowmetry.
Microvascular Research, 78(1):4–13.

Gallagher, A., Ní Annaidh, A., Bruyère, K., Otténio, M., Xie, H., and Gilchrist, M. (2012).
Dynamic tensile properties of human skin.
In *IRCOBI conference*, volume 59, pages 494–502. International Research Council on the Biomechanics of Injury Dublin (Ireland.

Gefen, A., Brienza, D. M., Cuddigan, J., Haesler, E., and Kottner, J. (2021).
Our contemporary understanding of the aetiology of pressure ulcers/pressure injuries.
International Wound Journal, n/a(n/a).

References

Gray, W. G. and Miller, C. T. (2014).
Introduction to the Thermodynamically Constrained Averaging Theory for Porous Medium Systems.
Springer International Publishing.

Greiner, A., Reiter, N., Paulsen, F., Holzapfel, G. A., Steinmann, P., Comellas, E., and Budday, S. (2021).
Poro-viscoelastic effects during biomechanical testing of human brain tissue.
Frontiers in Mechanical Engineering, 7.

Gunda, S., Natarajan, S., and Barrera, O. (2023).
On the fractional transversely isotropic functionally graded nature of soft biological tissues: Application to the meniscal tissue.
Journal of the Mechanical Behavior of Biomedical Materials, 143:105855.

Han, D., Huang, Z., Rahimi, E., and Ardekani, A. M. (2023).
Solute transport across the lymphatic vasculature in a soft skin tissue.
Biology, 12(7):942.

Hendriks, F. M., Brokken, D., Eemeren, J. T. W. M. V., Oomens, C. W. J., Baaijens, F. P. T., and Horsten, J. B. A. M. (2003).
A numerical-experimental method to characterize the non-linear mechanical behaviour of human skin.
Skin Research and Technology, 9(3):274–283.

References

Hervas-Raluy, S., Wirthl, B., Guerrero, P. E., Robalo Rei, G., Nitzler, J., Coronado, E., Font de Mora Sainz, J., Schrefler, B. A., Gomez-Benito, M. J., Garcia-Aznar, J. M., and Wall, W. A. (2023).
Tumour growth: An approach to calibrate parameters of a multiphase porous media model based on in vitro observations of neuroblastoma spheroid growth in a hydrogel microenvironment.
Computers in Biology and Medicine, 159:106895.

Hoskins, P. R., Lawford, P. V., and Doyle, B. J., editors (2017).
Cardiovascular Biomechanics.
Springer International Publishing.

Hosseini-Farid, M., Ramzanpour, M., McLean, J., Ziejewski, M., and Karami, G. (2020).
A poro-hyper-viscoelastic rate-dependent constitutive modeling for the analysis of brain tissues.
Journal of the Mechanical Behavior of Biomedical Materials, 102:103475.

Humphrey, J. D. and O'Rourke, S. L. (2015).
An Introduction to Biomechanics.
Springer New York.

Islam, M. R., Virag, J., and Oyen, M. L. (2020).
Micromechanical poroelastic and viscoelastic properties of ex-vivo soft tissues.
Journal of Biomechanics, 113:110090.

References

Jacquet, E., Chambert, J., Pauchot, J., and Sandoz, P. (2017).
Intra- and inter-individual variability in the mechanical properties of the human skin from in vivo measurements on 20 volunteers.
Skin Research and Technology, 23(4):491–499.

Joodaki, H. and Panzer, M. B. (2018).
Skin mechanical properties and modeling: A review.
Proceedings of the Institution of Mechanical Engineers, Part H: Journal of Engineering in Medicine, 232(4):323–343.

Jordan, P., Socrate, S., Zickler, T., and Howe, R. (2009).
Constitutive modeling of porcine liver in indentation using 3d ultrasound imaging.
Journal of the Mechanical Behavior of Biomedical Materials, 2(2):192–201.

Kaelo, P. and Ali, M. M. (2006).
Some variants of the controlled random search algorithm for global optimization.
Journal of Optimization Theory and Applications, 130(2):253–264.

Kalra, A. and Lowe, A. (2016).
Mechanical behaviour of skin: A review.
Journal of Material Science & Engineering, 5(4).

Kazemi, M., Dabiri, Y., and Li, L. P. (2013).
Recent advances in computational mechanics of the human knee joint.
Computational and Mathematical Methods in Medicine, 2013:1–27.

References

Khaothong, K. (2010).
In vivo measurements of the mechanical properties of human skin and muscle by inverse finite element method combined with the indentation test.
In *IFMBE Proceedings*, pages 1467–1470. Springer Berlin Heidelberg.

Khatyr, F., Imberdis, C., Vescovo, P., Varchon, D., and Lagarde, J.-M. (2004).
Model of the viscoelastic behaviour of skin in vivo and study of anisotropy.
Skin Research and Technology, 10(2):96–103.

Kim, J., Lee, J., and Lee, E. (2020).
Risk factors for newly acquired pressure ulcer and the impact of nurse staffing on pressure ulcer incidence.
Journal of Nursing Management, 30(5).

Kosiak, M. (1959).
Etiology and pathology of ischemic ulcers.
Arch Phys Med Rehabil, 40(2):62–69.

Lakhani, P., Dwivedi, K. K., Parashar, A., and Kumar, N. (2021).
Non-invasive in vivo quantification of directional dependent variation in mechanical properties for human skin.
Frontiers in Bioengineering and Biotechnology, 9.

Landis, E. M. (1930).
Micro-injection studies of capillary blood pressure in human skin.
Heart, 15:209–228.

References

Lavigne, T., Sciumè, G., Laporte, S., Pillet, H., Urcun, S., Wheatley, B., and Rohan, P.-Y. (2022).
Société de biomécanique young investigator award 2021: Numerical investigation of the time-dependent stress–strain mechanical behaviour of skeletal muscle tissue in the context of pressure ulcer prevention.
Clinical Biomechanics, 93:105592.

Lavigne, T., Urcun, S., Fromy, B., Josset-Lamaugarny, A., Lagache, A., Suarez-Afanador, C. A., Bordas, S. P. A., Rohan, P.-Y., and Sciumè, G. (2025).
Hierarchical poromechanical approach to investigate the impact of mechanical loading on human skin micro-circulation.
International Journal for Numerical Methods in Biomedical Engineering.

Lavigne, T., Urcun, S., Rohan, P.-Y., Sciumè, G., Baroli, D., and Bordas, S. P. (2023).
Single and bi-compartment poro-elastic model of perfused biological soft tissues: FEniCSx implementation and tutorial.
Journal of the Mechanical Behavior of Biomedical Materials, 143:105902.

Leng, Y., de Lucio, M., and Gomez, H. (2021).
Using poro-elasticity to model the large deformation of tissue during subcutaneous injection.
Computer Methods in Applied Mechanics and Engineering, 384:113919.

Loerakker, S., Manders, E., Strijkers, G. J., Nicolay, K., Baaijens, F. P. T., Bader, D. L., and Oomens, C. W. J. (2011).
The effects of deformation, ischemia, and reperfusion on the development of muscle damage during prolonged loading.
Journal of Applied Physiology, 111(4):1168–1177.

References

Lyon, C. C., Kulkarni, J., Zimersonc, E., Van Ross, E., and Beck, M. H. (2000).
Skin disorders in amputees.
Journal of the American Academy of Dermatology, 42(3):501–507.

Marchesseau, S., Heimann, T., Chatelin, S., Willinger, R., and Delingette, H. (2010).
Fast porous visco-hyperelastic soft tissue model for surgery simulation: Application to liver surgery.
Progress in Biophysics and Molecular Biology, 103(2–3):185–196.

Mellor, R. H., Bush, N. L., Stanton, A. W. B., Bamber, J. C., Levick, J. R., and Mortimer, P. S. (2004).
Dual-frequency ultrasound examination of skin and subcutis thickness in breast cancer-related lymphedema.
The Breast Journal, 10(6):496–503.

Meulenbelt, H. E., Geertzen, J. H., Jonkman, M. F., and Dijkstra, P. U. (2009).
Determinants of skin problems of the stump in lower-limb amputees.
Archives of Physical Medicine and Rehabilitation, 90(1):74–81.

Moore, Z., Avsar, P., Conaty, L., Moore, D. H., Patton, D., and O'Connor, T. (2019).
The prevalence of pressure ulcers in europe, what does the european data tell us: a systematic review.
Journal of Wound Care, 28(11):710–719.

Moran, E. C., Raghunathan, S., Evans, D. W., Vavalle, N. A., Sparks, J. L., LeRoith, T., and Smith, T. L. (2012).
Porohyperviscoelastic model simultaneously predicts parenchymal fluid pressure and reaction force in perfused liver.
Journal of Biomechanical Engineering, 134(9).

References

Morrow, D. A., Haut Donahue, T. L., Odegard, G. M., and Kaufman, K. R. (2012).
A poroelastic model of skeletal muscle tissue used to predict intramuscular pressure.
In *ASME 2012 Summer Bioengineering Conference, Parts A and B*, SBC2012, page 719–720. American Society of Mechanical Engineers.

Nakagawa, N., Matsumoto, M., and Sakai, S. (2010).
In vivo measurement of the water content in the dermis by confocal raman spectroscopy.
Skin Research and Technology, 16(2):137–141.

Oftadeh, R., Azadi, M., Donovan, M., Langer, J., Liao, I.-C., Ortiz, C., Grodzinsky, A. J., and Luengo, G. S. (2023).
Poroelastic behavior and water permeability of human skin at the nanoscale.
PNAS Nexus, 2(8).

Oftadeh, R., Connizzo, B. K., Nia, H. T., Ortiz, C., and Grodzinsky, A. J. (2018).
Biological connective tissues exhibit viscoelastic and poroelastic behavior at different frequency regimes: Application to tendon and skin biophysics.
Acta Biomaterialia, 70:249–259.

Oomens, C., van Campen, D., and Grootenboer, H. (1987).
A mixture approach to the mechanics of skin.
Journal of Biomechanics, 20(9):877–885.

Ottenio, M., Tran, D., Annaidh, A. N., Gilchrist, M. D., and Bruyère, K. (2015).
Strain rate and anisotropy effects on the tensile failure characteristics of human skin.
Journal of the Mechanical Behavior of Biomedical Materials, 41:241–250.

References

Pailler-Mattei, C., Bec, S., and Zahouani, H. (2008).
In vivo measurements of the elastic mechanical properties of human skin by indentation tests.
Medical Engineering & Physics, 30(5):599–606.

Parvizi, A., Haddadi, S., Mollaei, A., Ghorbani Vajargah, P., Takasi, P., Firooz, M., Hosseini, S. J., Farzan, R., and Karkhah, S. (2023).
A systematic review of nurses' knowledge and related factors towards the prevention of medical device-related pressure ulcers.
International Wound Journal, 20(7):2843–2854.

Pence, T. J. and Gou, K. (2014).
On compressible versions of the incompressible neo-hookean material.
Mathematics and Mechanics of Solids, 20(2):157–182.

Raghunathan, S., Evans, D., and Sparks, J. L. (2010).
Poroviscoelastic modeling of liver biomechanical response in unconfined compression.
Annals of Biomedical Engineering, 38(5):1789–1800.

Raveh Tilleman, T., Tilleman, M., and Neumann, H. (2004).
The elastic properties of cancerous skin: Poisson's ratio and young's modulus.
Optimization of Incisions in Cutaneous Surgery including Mohs' Micrographic Surgery, 105(2).

Ricken, T. and Lambers, L. (2019).
On computational approaches of liver lobule function and perfusion simulation.
GAMM-Mitteilungen, 42(4).

References

Sachs, D., Jakob, R., Restivo, G., Hafner, J., Lindenblatt, N., Ehret, A. E., and Mazza, E. (2024).
A quadriphasic mechanical model of the human dermis.
Biomechanics and Modeling in Mechanobiology, 23(4):1121–1136.

Sachs, D., Wahlsten, A., Kozerke, S., Restivo, G., and Mazza, E. (2021).
A biphasic multilayer computational model of human skin.
Biomechanics and Modeling in Mechanobiology, 20(3):969–982.

Samant, P. P. and Prausnitz, M. R. (2018).
Mechanisms of sampling interstitial fluid from skin using a microneedle patch.
Proceedings of the National Academy of Sciences, 115(18):4583–4588.

Sanders, R. (1973).
Torsional elasticity of human skin in vivo.
Pfl gers Archiv European Journal of Physiology, 342(3):255–260.

Schwer, J., Galbusera, F., Ignatius, A., Dürselen, L., and Seitz, A. M. (2024).
Non-invasive regional parameter identification of degenerated human meniscus.
Computers in Biology and Medicine, 182:109230.

Sciumè, G. (2021).
Mechanistic modeling of vascular tumor growth: an extension of biot's theory to hierarchical bi-compartment porous medium systems.
Acta Mechanica, 232(4):1445–1478.

References

Sciumè, G., Boso, D. P., Gray, W. G., Cobelli, C., and Schrefler, B. A. (2014).
A two-phase model of plantar tissue: a step toward prediction of diabetic foot ulceration.
International Journal for Numerical Methods in Biomedical Engineering, 30(11):1153–1169.

Sowinski, D. R., McGarry, M. D. J., Houten, E. E. W. V., Gordon-Wylie, S., Weaver, J. B., and Paulsen, K. D. (2021).
Poroelasticity as a model of soft tissue structure: Hydraulic permeability reconstruction for magnetic resonance elastography in silico.
Frontiers in Physics, 8.

Sree, V. D., Rausch, M. K., and Tepole, A. B. (2019).
Towards understanding pressure ulcer formation: Coupling an inflammation regulatory network to a tissue scale finite element model.
Mechanics Research Communications, 97:80–88.

Stekelenburg, A., Oomens, C. W. J., Strijkers, G. J., Nicolay, K., and Bader, D. L. (2006).
Compression-induced deep tissue injury examined with magnetic resonance imaging and histology.
Journal of Applied Physiology, 100(6):1946–1954.

Stracuzzi, A., Mazza, E., and Ehret, A. E. (2018).
Chemomechanical models for soft tissues based on the reconciliation of porous media and swelling polymer theories.
ZAMM - Journal of Applied Mathematics and Mechanics / Zeitschrift für Angewandte Mathematik und Mechanik, 98(12):2135–2154.

Su, L., Wang, M., Yin, J., Ti, F., Yang, J., Ma, C., Liu, S., and Lu, T. J. (2023).
Distinguishing poroelasticity and viscoelasticity of brain tissue with time scale.
Acta Biomaterialia, 155:423–435.

References

Swisher, S. L., Lin, M. C., Liao, A., Leeflang, E. J., Khan, Y., Pavinatto, F. J., Mann, K., Naujokas, A., Young, D., Roy, S., Harrison, M. R., Arias, A. C., Subramanian, V., and Maharbiz, M. M. (2015).
Impedance sensing device enables early detection of pressure ulcers in vivo.
Nature Communications, 6(1).

Torres-Terán, I., Venczel, M., Stieler, T., Parisi, L., Kloss, A., and Klein, S. (2023).
Prediction of subcutaneous drug absorption - characterization of subcutaneous interstitial fluids as a basis for developing biorelevant in vitro models.
International Journal of Pharmaceutics, 638:122906.

Traa, W. A., van Turnhout, M. C., Nelissen, J. L., Strijkers, G. J., Bader, D. L., and Oomens, C. W. (2019).
There is an individual tolerance to mechanical loading in compression induced deep tissue injury.
Clinical Biomechanics, 63:153–160.

Urcun, S., Baroli, D., Rohan, P.-Y., Skalli, W., Lubrano, V., Bordas, S. P., and Sciume, G. (2023).
Non-operable glioblastoma: proposition of patient-specific forecasting by image-informed poromechanical model.
Brain Multiphysics, page 100067.

Urcun, S., Rohan, P.-Y., Sciumè, G., and Bordas, S. P. (2022).
Cortex tissue relaxation and slow to medium load rates dependency can be captured by a two-phase flow poroelastic model.
Journal of the Mechanical Behavior of Biomedical Materials, 126:104952.

References

Urcun, S., Rohan, P.-Y., Skalli, W., Nassoy, P., Bordas, S. P. A., and Sciumè, G. (2021).
Digital twinning of cellular capsule technology: Emerging outcomes from the perspective of porous media mechanics.
PLOS ONE, 16(7):e0254512.

Uzuner, S., Kuntze, G., Li, L., Ronsky, J., and Kucuk, S. (2022).
Creep behavior of human knee joint determined with high-speed biplanar video-radiography and finite element simulation.
Journal of the Mechanical Behavior of Biomedical Materials, 125:104905.

Uzuner, S., Li, L., Kucuk, S., and Memisoglu, K. (2020).
Changes in knee joint mechanics after medial meniscectomy determined with a poromechanical model.
Journal of Biomechanical Engineering, 142(10).

Vanderwee, K., Clark, M., Dealey, C., Gunningberg, L., and Defloor, T. (2007).
Pressure ulcer prevalence in europe: a pilot study.
Journal of Evaluation in Clinical Practice, 13(2):227–235.

Wahlsten, A., Pensalfini, M., Stracuzzi, A., Restivo, G., Hopf, R., and Mazza, E. (2019).
On the compressibility and poroelasticity of human and murine skin.
Biomechanics and Modeling in Mechanobiology, 18(4):1079–1093.

Wahlsten, A., Stracuzzi, A., Lüchtefeld, I., Restivo, G., Lindenblatt, N., Giampietro, C., Ehret, A. E., and Mazza, E. (2023).
Multiscale mechanical analysis of the elastic modulus of skin.
Acta Biomater., 170:155–168.

References

Wang, M., Liu, S., Xu, Z., Qu, K., Li, M., Chen, X., Xue, Q., Genin, G. M., Lu, T. J., and Xu, F. (2020).
Characterizing poroelasticity of biological tissues by spherical indentation: An improved theory for large relaxation.
Journal of the Mechanics and Physics of Solids, 138:103920.

Weir Weiss, M.-J., Shrestha, P., Basak, R., and Stoeber, B. (2023).
Poroelastic behavior of skin tissue in response to pressure driven flow.
Physics of Fluids, 35(8):081902.

Wheatley, B. B., Fischenich, K. M., Button, K. D., Haut, R. C., and Haut Donahue, T. L. (2015).
An optimized transversely isotropic, hyper-poro-viscoelastic finite element model of the meniscus to evaluate mechanical degradation following traumatic loading.
Journal of Biomechanics, 48(8):1454–1460.

Wheatley, B. B., Odegard, G. M., Kaufman, K. R., and Haut Donahue, T. L. (2016).
A case for poroelasticity in skeletal muscle finite element analysis: experiment and modeling.
Computer Methods in Biomechanics and Biomedical Engineering, 20(6):598–601.

Wiig, H. and Swartz, M. A. (2012).
Interstitial fluid and lymph formation and transport: Physiological regulation and roles in inflammation and cancer.
Physiological Reviews, 92(3):1005–1060.

Wong, R., Geyer, S., Weninger, W., Guimberteau, J.-C., and Wong, J. K. (2015).
The dynamic anatomy and patterning of skin.
Experimental Dermatology, 25(2):92–98.

References

Yang, M. and Taber, L. A. (1991).
The possible role of poroelasticity in the apparent viscoelastic behavior of passive cardiac muscle.
Journal of Biomechanics, 24(7):587–597.

Yazdi, S. J. M. and Baqersad, J. (2022).
Mechanical modeling and characterization of human skin: A review.
Journal of Biomechanics, 130:110864.